EPA-600/2-77-009
January 1977

Environmental Protection Technology Series

CARBON DIOXIDE LASER SYSTEM TO MEASURE GASEOUS POLLUTANTS

Environmental Sciences Research Laboratory
Office of Research and Development
U.S. Environmental Protection Agency
Research Triangle Park, North Carolina 27711

RESEARCH REPORTING SERIES

Research reports of the Office of Research and Development, U.S. Environmental Protection Agency, have been grouped into five series. These five broad categories were established to facilitate further development and application of environmental technology. Elimination of traditional grouping was consciously planned to foster technology transfer and a maximum interface in related fields. The five series are:

1. Environmental Health Effects Research
2. Environmental Protection Technology
3. Ecological Research
4. Environmental Monitoring
5. Socioeconomic Environmental Studies

This report has been assigned to the ENVIRONMENTAL PROTECTION TECHNOLOGY series. This series describes research performed to develop and demonstrate instrumentation, equipment, and methodology to repair or prevent environmental degradation from point and non-point sources of pollution. This work provides the new or improved technology required for the control and treatment of pollution sources to meet environmental quality standards.

This document is available to the public through the National Technical Information Service, Springfield, Virginia 22161.

EPA-600/7-77-009
January 1977

CARBON DIOXIDE LASER SYSTEM TO MEASURE GASEOUS POLLUTANTS

by

R.J. Gillmeister and L.R. Snowman
General Electric
Pittsfield, Massachusetts 01201

Contract No. 68-02-1290

Project Officer

William A. McClenny
Atmospheric Instrumentation Branch
Environmental Sciences Research Laboratory
Research Triangle Park, NC 27711

ENVIRONMENTAL SCIENCES RESEARCH LABORATORY
OFFICE OF RESEARCH AND DEVELOPMENT
U.S. ENVIRONMENTAL PROTECTION AGENCY
RESEARCH TRIANGLE PARK, NC 27711

DISCLAIMER

This report has been reviewed by the Environmental Sciences Research Laboratory, U.S. Environmental Protection Agency, and approved for publication. Approval does not signify that the contents necessarily reflect the views and policies of the U.S. Environmental Protection Agency, nor does mention of trade names or commercial products constitute endorsement or recommendation for use.

ABSTRACT

Reported here is the continuation of work in the development of a gas laser system for air pollution monitoring over long paths, a kilometer or more, using infrared absorption. Discussed are modifications to a breadboard system for simultaneous detection of ozone, ammonia and ethylene and the addition of beam steering optics to give the system area monitoring capability. Operation for a two month period in St. Louis in conjunction with the RAPS program is also discussed. Data comparing system performance with that of conventional monitors is presented along with the results of problem investigations. While reasonable correlation with point monitor results is indicated, it is concluded that system performance can be improved. Recommendations are given for further activity to achieve better system performance.

CONTENTS

LIST OF FIGURES

LIST OF TABLES

ACKNOWLEDGEMENTS

The authors wish to gratefully acknowledge the support of many people in obtaining the results reported here. In particular we thank W. S. Beeman, S. E. Craig, J. B. Haberl, A. J. Nesti, J. Ozolins and D. L. Roberts.

Section I

CONCLUSIONS

Contract 68-02-1290 specified modifications of ILAMS (Infrared Laser Atmospheric Monitoring System) and its operation in St. Louis in conjunction with the RAPS program. The modifications, the change to a six wavelength configuration was the largest of these, were intended principally to extend the system's pollutant monitoring capability to three target gases, ozone, ammonia and ethylene. Beam steering capability, to permit positioning of the beam, 360° in azimuth and ±10° in elevation was also added. Analysis and measurement of causes contributing to system errors noted in earlier field tests were begun and useful information obtained. Progress was made in improving system performance, but resource constraints limited what could be done in this area.

In St. Louis, useful field experience was gained operating in a rather severe environment. The system was operated over several paths, two of them about 500 meters in range (one way distance). The last one exceeded 900 meters range, with much of it over a two lane concrete highway. A fertilizer plant, emitting large amounts of ammonia and particulates, was located along the path.

While the data show reasonable correlation between the path and point monitor instruments, there is room for improvement in the performance of the system. Data review and analysis indicates:

1) Optical effects on the six wavelength beam pattern are a principal source of error.

2) Changes in signal processing can significantly reduce short term excursions in ozone concentration measurements.

3) Spectral effects not factored into the wavelength selection process were a source of error occurring under certain conditions.

4) Zeroing of the system, independent of other instruments, is an important feature which must be incorporated to eliminate errors.

Section II

RECOMMENDATIONS

A concerted effort to address system problems with the objective of achieving its full performance potential is an essential next step in the development of ILAMS.

A large amount of measurement data has been accumulated. Because this data exists and because the system can be precisely modeled both as to the electronic and optical signal processing a quantitative system error analysis can now be performed. It should be conducted to give direction to error reduction activities. It will point out the nature and magnitude of the sources of system error and provide the basis for specific design recommendations. These design changes should be incorporated in the system and its performance evaluated in field measurements to determine results achieved.

Section III

INTRODUCTION

A gas laser system to measure trace gases by long path absorption techniques has been under development for some time. Called ILAMS, it is described in Appendix A. Briefly, a flowing gas CO_2 laser is uniquely configured to produce multiple wavelengths which are transmitted in a rapid sequence to a distant retroreflector. The retro returns incident energy to an off-axis parabola which serves as both the transmit and receive optical element. In the signal processor, the natural logarithm of the return to transmitted signal ratio is taken for each wavelength. These logs are weighted and summed to produce an output proportional to pollutant concentration in accordance with Beer's Law principles. Transmitted wavelengths are selected with the aid of computer programs using absorption coefficient data for target gases and expected spectral interferences, to maximize return signal to noise ratios. Linear weights are computer-calculated to discriminate pollutant effects from interferences.

Under this contract the system was modified for simultaneous detection of O_3, NH_3 and C_2H_4. This required changes to the laser dictated by the wavelength selection process; a six wavelength configuration was selected for the detection problem. New linear weights were determined. Certain other laser modifications were also made. Beam steering optics were added to the system so that it could be operated over multiple paths in a fairly rapid sequence. The beam can be steered through 360° in azimuth and approximately ±10° in elevation. The system was transported to St. Louis and operated there for a two month period, mid-August thru early October 1974, in conjunction with the RAPS program. The drift problem, first identified under

Contract 68-02-0757, is evident in the data. Time and dollar constraints of the program permitted only limited study of the problem, but useful information was obtained. The work is described in the sections which follow. The last section, Discussion, reviews the field measurement results and presents some analysis of the data.

Section IV

SYSTEM MODIFICATIONS

SIGNAL PROCESSING

ILAMS measures directly the transmission (T_1, T_2, T_3, ... T_n) of the sample region between the transmitter and the retroreflector at n selected wavelengths. Assuming that the line width of the resonance absorption is broad compared to the transmitted laser line width, and assuming also that there is no saturation in the absorbing media, then, for a uniform concentration of the absorber over the path, the transmission at each discrete wavelength is of the form, $T_m = \exp(-A_m C_A L)$; where A_m is the absorption coefficient of absorber A at wavelength m, C_A is the concentration of absorber A over the total optical path, and L is the total optical path through the sample region. If the concentration is non-uniform over the path, as is the more usual case, then $C_A L$ can be replaced by the integrated concentration over the path.

Typically, C has units of grams/liter or atmospheres of partial pressure, and L is in centimeters. A_m is in units to make $A_m C_A L$ dimensionless.

If a second absorber B with absorption coefficients B_m is introduced into the region, the net transmission will be the product of the transmission due to each absorber.

$$T_m = e^{-(A_m C_A L + B_m C_B L)}$$

If the natural log of the transmission at each wavelength is taken electronically, then

$$S_m \triangleq \ln T_m = -(A_m C_A L + B_m C_B L) \qquad (2)$$

and the resulting signals have two convenient properties:

1) System response to any absorber is a linear function of the quantity (concentration x path) present

2) System response to several absorbers is the sum of the responses to the individual absorbers.

Therefore, if the system can be designed to give a zero response to spectrally interfering absorbers, the system will respond only to the pollutant to be measured, and the response will be proportional to the quantity present.

Speaking more generally, the above properties define a linear n-dimensional vector space. Each gas is represented by a vector in this space whose length is proportional to the concentration. This formalization permits the application of known mathematical and statistical techniques.

Using decision theory and multivariate statistical analysis, it can be shown that the optimum signal processing involves the use of single or multiple linear weights. Application of a single linear weight, W, means taking a linear sum of the signals $S_1, S_2, \ldots S_n$ to give a new signal, $S = W_1 S_1 + W_2 S_2 + \ldots W_n S_n$. The quantity of absorbers present can be accurately determined by examining the magnitude of such linear sums.

Techniques may also be applied for choosing linear weights to accurately measure the quantity of a given pollutant in the presence of known interfering spectral absorbers, random spectral absorbers, scintillation,

and other "noises". A definitive study on spectral absorption pattern detection and estimation techniques using linear weights appears in Reference 2. A summary of the applicable results is given in Appendices A and B of Reference 1.

Gas lasers offer a large number of lines from which wavelengths can be selected to detect practically all important pollutants (See Appendix B and Reference 3.) On the basis of both analytical and experimental work, several basic conclusions about wavelength selection can be drawn.

1) The relative success of a group of wavelengths depends directly on the measurement problem. The pollutants to be measured, pollutants and absorbers to be ignored, expected quantities of absorbers and the system noise levels, all affect the choice of wavelengths.

2) For a given problem, there will be an optimum set of wavelengths. Increasing the number of pollutants to be estimated or ignored will tend to increase the optimum number of wavelengths to be used; i.e., the more complex the environment, the more wavelengths are necessary.

3) The finer the spectral structure of an absorber, the fewer number of wavelengths are needed to best measure the quantities of it present. The laser system is not limited to detecting pollutants with fine structure such as ammonia and ethylene. In fact, it does remarkably well in detecting or rejecting absorbers with rather smooth spectral characteristics.

The primary target gases in this program were ozone, ammonia and ethylene. Carbon dioxide, water vapor and neutral attenuation were the interferences considered for these targets. For a single target gas, past experience has shown that four wavelengths have done an excellent job in handling spectral recognition problems in environments representative of the real world. However, for this program, a six wavelength configuration was selected because of the relative complexity of the detection problem. In Reference 1, the general topics of Interferences and Optimum Linear Weights are discussed, respectively, in Appendices A and B. A systematical approach to the wavelength selection problem using mathematical and computer techniques is presented in Appendix C.

Wavelength Selection

In Appendix C of Reference 1 the philosophy and methodology of wavelength selection is delineated as a two step computer-aided process. In order to reduce the possibility of problems associated with proximity of water vapor absorption lines, a number of CO_2 laser lines were eliminated from consideration before proceeding with the computerized wavelength selection process. Table 1 lists the potentially troublesome water vapor lines and nearby laser lines together with calculated absorption coefficients at the laser line center. Data on water vapor was taken from Stanford Research Institute computer printouts. A preliminary wavelength selection was then made to reduce the number of potential CO_2 laser lines from 59 to 20 by using a computer program called LWSP. This program eliminates wavelengths of low information by an iteration process of adjusting the power allocation. The second step in the selection process involves a combinatorial evaluation of the reduced set by which all combinations are ranked in accordance with their performance in measuring ozone, ethylene and ammonia. An existing program (MFIL) was modified to perform this operation and is called CMFIL.

Table 1

WATER VAPOR - CO_2 LASER LINE INTERFERENCE DATA

H_2O Line (cm^{-1})	Width (cm^{-1})	α ($atm^{-1}\ cm^{-1}$)	CO_2 Laser Line (cm^{-1})	α @ Laser Line ($atm^{-1}\ cm^{-1}$)	J Value	Relative Importance
924.988	.050	1.59×10^{-3}	924.975	1.25×10^{-3}	P-40	1
929.071	.048	1.98×10^{-4}	929.018	3.37×10^{-5}	P-36	6
970.644	.040	1.89×10^{-4}	970.548	7.84×10^{-6}	R-12	11
976.012	.040	1.57×10^{-3}	975.931	9.02×10^{-5}	R-20	4
973.486	.034	8.20×10^{-4}	973.289	6.06×10^{-6}	R-16	13
977.420	.064	4.80×10^{-4}	977.215	1.17×10^{-5}	R-22	10
1029.490	.041	1.02×10^{-3}	1029.442	1.57×10^{-4}	P-38	3
1039.470	.052	3.90×10^{-4}	1039.369	2.42×10^{-5}	P-28	9
1055.500	.061	5.55×10^{-4}	1055.625	3.12×10^{-5}	P-10	7
1066.200	.047	7.00×10^{-3}	1066.037	8.82×10^{-4}	R-02	2
1073.315	.027	6.10×10^{-5}	1073.278	7.17×15^{-6}	R-12	12
1074.430	.050	2.21×10^{-3}	1074.646	2.92×10^{-5}	R-14	8
1091.240	.056	2.99×10^{-3}	1091.031	5.27×10^{-5}	R-42	5

A 25 iteration LWSP run resulted in the preliminary line selections for each target illustrated in Figures 1 through 3. The solid lines in these figures represent the linear weights applied to each wavelength and their length is indicative of the relative importance of each line. The X's designate normalized ozone absorption coefficients and the +'s designate the average interferent noise level.

The top 10 wavelengths from the LWSP output were selected to form the basis set for CMFIL. Combinations of this set were then evaluated and ranked using CMFIL. The output listing for the three targets is shown in Figure 4. The combination 1, 2, 3, 7, 9 & 10 (circled in the Figure) was selected as the one that gave the best compromise between the highest signal-to-noise-ratio (SNR) and ease of implementation in the laser. It can be seen from Figure 4 that the SNR penalty in the selected combination is small.

Linear Weight Computation

After the six wavelengths were selected, the optimum linear weights for measuring each of the target and interferent species were computed using the MFIL program. The absorption coefficients for the selected lines are shown in Table 2. For the present detection problem the mutual interference of O_3, H_2O, CO_2, C_2H_4 and NH_3 was modeled by the covariance matrix approach as implemented in MFIL. Scintillation and detector noise were treated as a single, uncorrelated noise source. Since neutral attenuation is a dominant interference and is not very statistically well-behaved or modeled, the weights were orthogonally constrained to reject this interference, i.e.,

$$W_1 + W_2 + W_3 + W_4 + W_5 + W_6 = 0$$

for each target. This was indirectly accomplished by assigning a large variance to neutral attenuation (as well as to targets and interferences), see Table 2. The linear weights obtained are shown in Table 3. Their cross responses are given in Table 4.

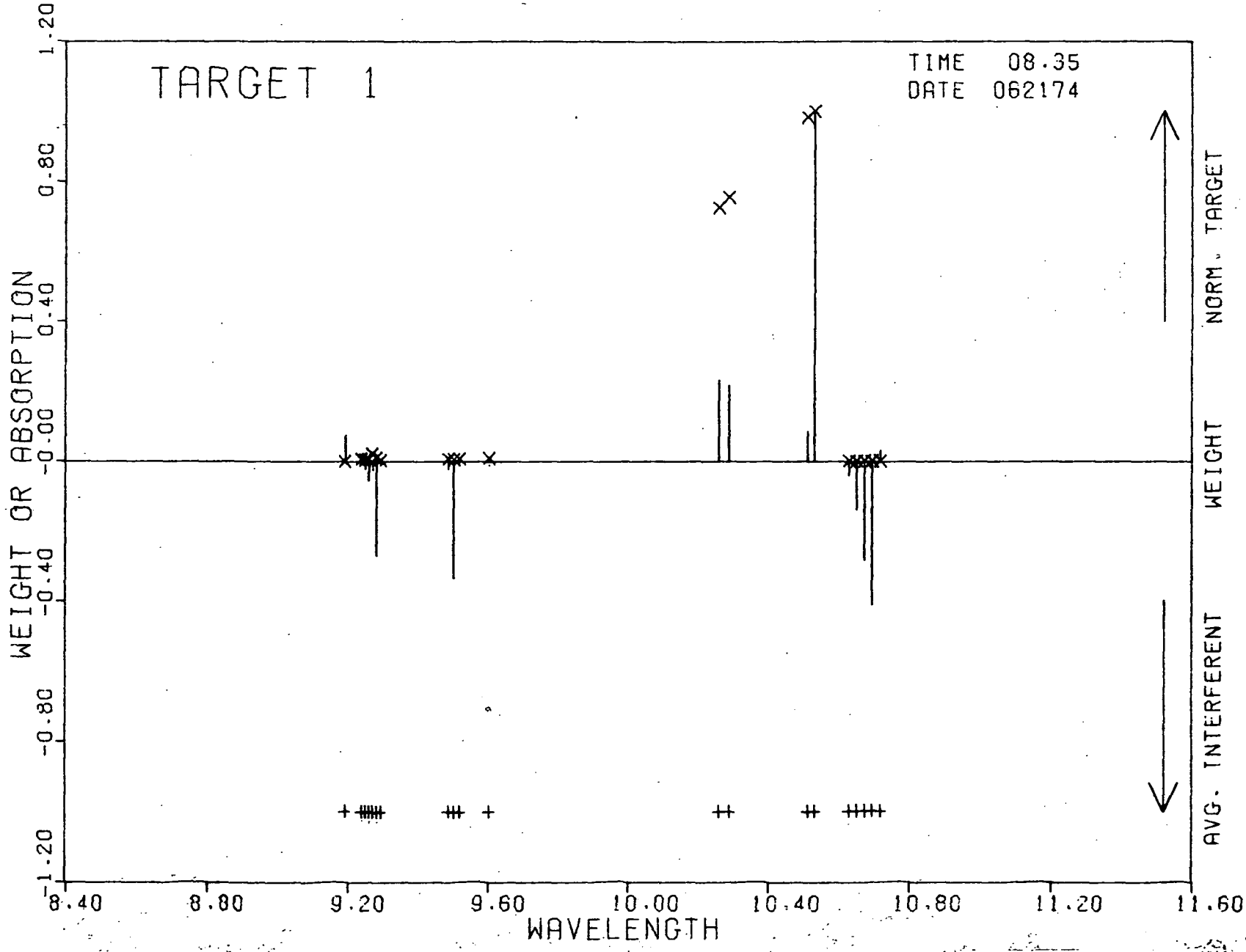

Figure 1. RESULTANT ETHYLENE LINE SELECTION FROM 25 ITERATION LWSP RUN

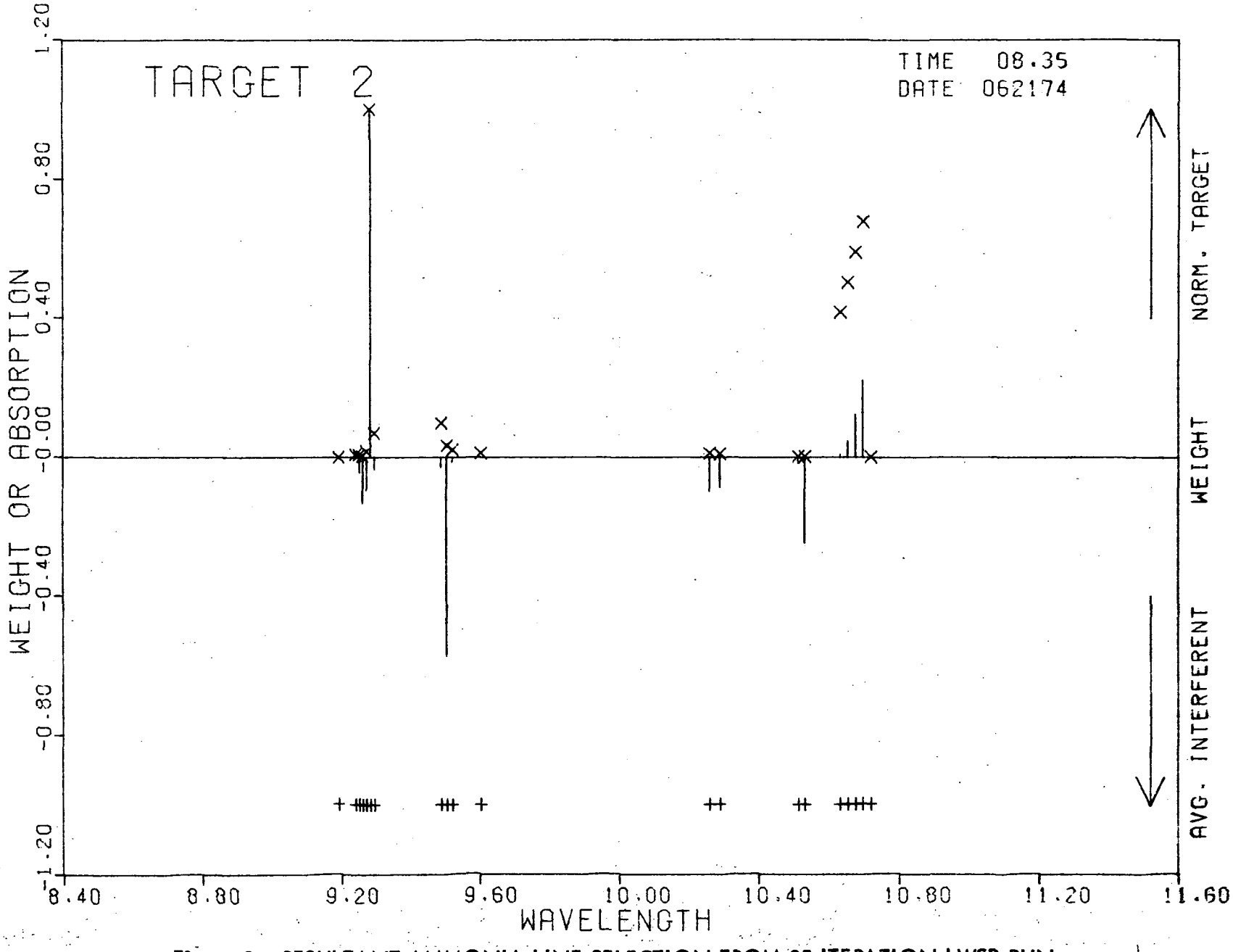

Figure 2. RESULTANT AMMONIA LINE SELECTION FROM 25 ITERATION LWSP RUN

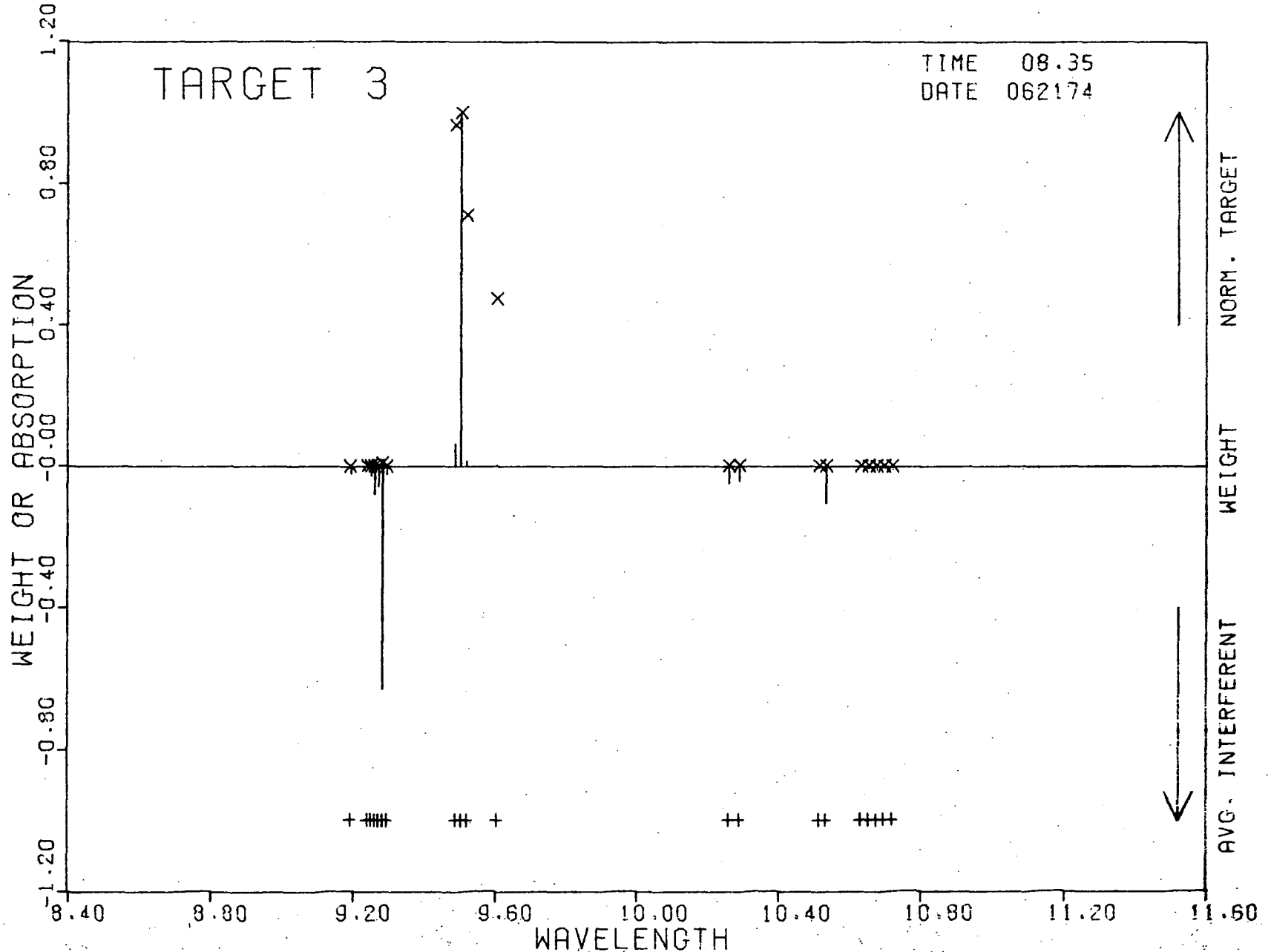

Figure 3. RESULTANT OZONE LINE SELECTION FROM 25 ITERATION LWSP RUN

COMBINATIONS OF 10 WAVELENGTHS, 6 AT A TIME, USING 1 THROUGH 10*

1	2	3	4	5	6	7	8	9	10
9.249900	9.290800	9.505700	10.333700	10.476000	10.494500	10.532100	10.591000	10.632100	10.696400
1031.092773	1076.980145	1052.129615	967.707603	954.562813	952.880074	949.478264	944.197906	940.547966	934.893982

SUM	WAVELENGTHS																	
333.03301	2	3	4	5	6	0												
315.46305	1	2	3	7	9	10	283.34100	1	3	4	6	7	8	117.84003	2	3	5	6	7	9
313.30420	1	3	4	7	8	10	282.89109	1	3	4	5	6	7	116.27672	2	3	4	5	6	9
313.27819	1	2	3	7	8	10	263.65334	1	3	5	7	8	10	116.17893	3	4	5	6	7	9
305.20800	1	2	3	5	8	10	263.31756	1	3	5	8	9	10	113.13588	3	4	5	6	7	10
301.87397	1	2	3	4	8	9	256.07702	1	3	5	7	9	10	106.88219	2	1	1	6	9	10
300.45103	1	2	3	8	9	10	256.00804	1	3	5	6	9	10	105.65019	2	3	4	8	9	10
299.98512	1	2	3	5	9	10	254.13359	1	3	7	8	9	10	84.86986	3	5	6	7	8	10
299.11207	1	2	3	4	5	6	253.83157	1	3	6	7	9	10	82.03304	1	3	4	7	8	9
290.09062	1	2	3	4	6	8	252.87314	1	3	5	6	7	10	79.31270	3	5	6	7	8	9
298.81707	1	2	3	4	9	10	251.46286	1	3	5	6	8	10	75.13602	1	3	5	6	7	9
298.00067	1	2	3	4	8	10	223.50657	1	3	6	7	8	10	48.03009	1	3	5	6	8	9
297.94690	1	2	3	6	7	10	217.59459	2	3	7	8	9	10	43.03641	1	3	5	6	7	8
297.68326	1	2	3	4	6	7	213.58671	1	3	6	8	9	10	33.66413	1	3	6	7	8	9
297.27602	1	2	3	5	7	8	209.35777	3	4	7	8	9	10	0.	1	4	5	6	7	10
297.21180	1	3	4	5	8	10	208.34166	2	3	6	7	9	10	0.	1	2	4	5	6	9
296.71113	1	2	3	5	7	9	207.09418	2	3	4	7	8	10	0.	1	4	5	8	9	10
296.25343	1	3	4	7	9	10	206.29518	3	4	6	7	9	10	0.	1	4	5	6	7	8
296.25154	1	3	4	5	8	9	202.81506	2	3	4	7	9	10	0.	1	2	4	8	9	10
295.95622	1	3	4	6	8	10	201.75308	2	3	5	7	8	10	0.	1	5	6	8	9	10
295.68015	2	3	4	5	9	10	190.20189	2	3	4	6	7	8	0.	1	2	4	6	8	10

*This is a partial listing of the original listing.
This modification has been made to facilitate
reproduction of this manuscript.

Figure 4. CMFIL OUTPUT LISTING

Species	ABSORPTION COEFFICIENT $ATM^{-1}\ CM^{-1}$ Laser Wavelengths (Microns) 9.2499	9.2938	9.5039	10.5321	10.6321	10.6964	Variance $(CL)^2$
O_3	0.	0.	12.7000	0.	0.	0.	100
CO_2	0.0035	0.0040	0.0035	0.0023	0.0021	0.0013	100
C_2H_4	0.1800	0.2800	0.1400	29.1000	2.1000	1.6300	100
NH_3	0.0640	12.7000	0.3100	0.8100	0.1300	0.8600	100
H_2O	0.0001	0.0001	0.0001	0.0002	0.0002	0.0002	100
Neutral Atten.	1.0000	1.0000	1.0000	1.0000	1.0000	1.0000	100

Table 2 ABSORPTION COEFFICIENTS AND CL VARIANCE OF ATMOSPHERIC SPECIES

LINEAR WEIGHTS

Species	Laser Wavelengths (Microns) 9.2499	9.2938	9.5039	10.5321	10.6321	10.6964	Relative SNR
O_3	-0.5655	-0.0527	1.0000	0.0388	-0.9946	0.5741	324.18
CO_2	1.0000	0.0482	0.0000	0.0605	-0.3133	-0.7954	0.047
C_2H_4	-0.3006	-0.0351	-0.0000	1.0000	-0.3092	-0.3551	801.62
NH_3	-1.0000	0.8897	-0.0000	-0.0044	-0.2748	0.3895	265.96
H_2O	-0.4566	0.0308	-0.0000	-0.0397	1.0000	-0.5345	0.0005
Neutral Atten.	-0.6624	-0.0329	-0.0000	-0.0943	1.0000	0.4734	16.86

Table 3 LINEAR WEIGHTS AND SNR'S FOR ATMOSPHERIC SPECIES

TARGET GAS - INTERFERENCE CROSS RESPONSES

Species	O_3	CO_2	C_2H_4	NH_3	H_2O	Neutral
O_3	12.7	5.7×10^{-5}	3.4×10^{-4}	3.7×10^{-4}	-3.8×10^{-5}	0.0
CO_2	0.0	21.4×10^{-4}	3.9×10^{-4}	3.7×10^{-4}	-1.0×10^{-4}	0.0
C_2H_4	0.0	-3.4×10^{-6}	27.8	-5.9×10^{-4}	3.4×10^{-5}	0.0
NH_3	0.0	-2.2×10^{-5}	-11.2×10^{-4}	11.53	1.1×10^{-5}	0.0
H_2O	0.0	1.6×10^{-4}	-6.9×10^{-5}	1.1×10^{-4}	4.3×10^{-5}	0.0
Neutral	0.0	4.9×10^{-5}	9.3×10^{-4}	5.2×10^{-4}	2×10^{-4}	0.0

Table 4 CROSS RESPONSE OF LINEAR WEIGHTS

LASER MODIFICATIONS

Adopting six wavelengths for the pollutant detection problem was the principal impetus for change to the laser configuration shown in Figure 33 Appendix A. Changes in optical elements external to the laser cavity (beam propagation optics) were made to improve system performance. In the spectrally scanning laser, rapid sequential transmission of several wavelengths is achieved using the concept diagrammed in Figure 5. The grating disperses the laser beam into its wavelength components. The mirrors between the grating and the chopper wheel are positioned to intercept the wavelengths selected and direct them through the chopper wheel to the end mirrors. The chopper wheel, rotating at about 40 Hz (in this instance) serves to "chop" the laser beam for detection purposes and also permits but one of the selected wavelengths to lase at a time. Originally in a four wavelength configuration, the change to six wavelengths required a new end mirror mount with two additional end mirrors, a new chopper wheel, repositioning of the intermediate mirrors and re-alignment of the mirror system. Coincidentally, a solid aluminum grating was installed, replacing the resin base grating that was showing signs of waxing under the high density laser beam.

Changes in beam propagation optics were made concurrently with laser modifications and later, during St. Louis field operations. Experiments (see Section VI) had shown that the beam splitter was seriously degrading the beam configuration produced by the spatial filter. It was replaced. However, the variation in concentration readout as observed on the teletype printout still exceeded that obtained the previous fall in a four wavelength configuration. Satisfactory readout stability was achieved with the introduction of a second pinhole at the focal point of the Ge focussing lens, between the lens and the collimator (see fig. 33). This performance could not be duplicated in St. Louis, however, and ultimately the second pinhole was removed, the

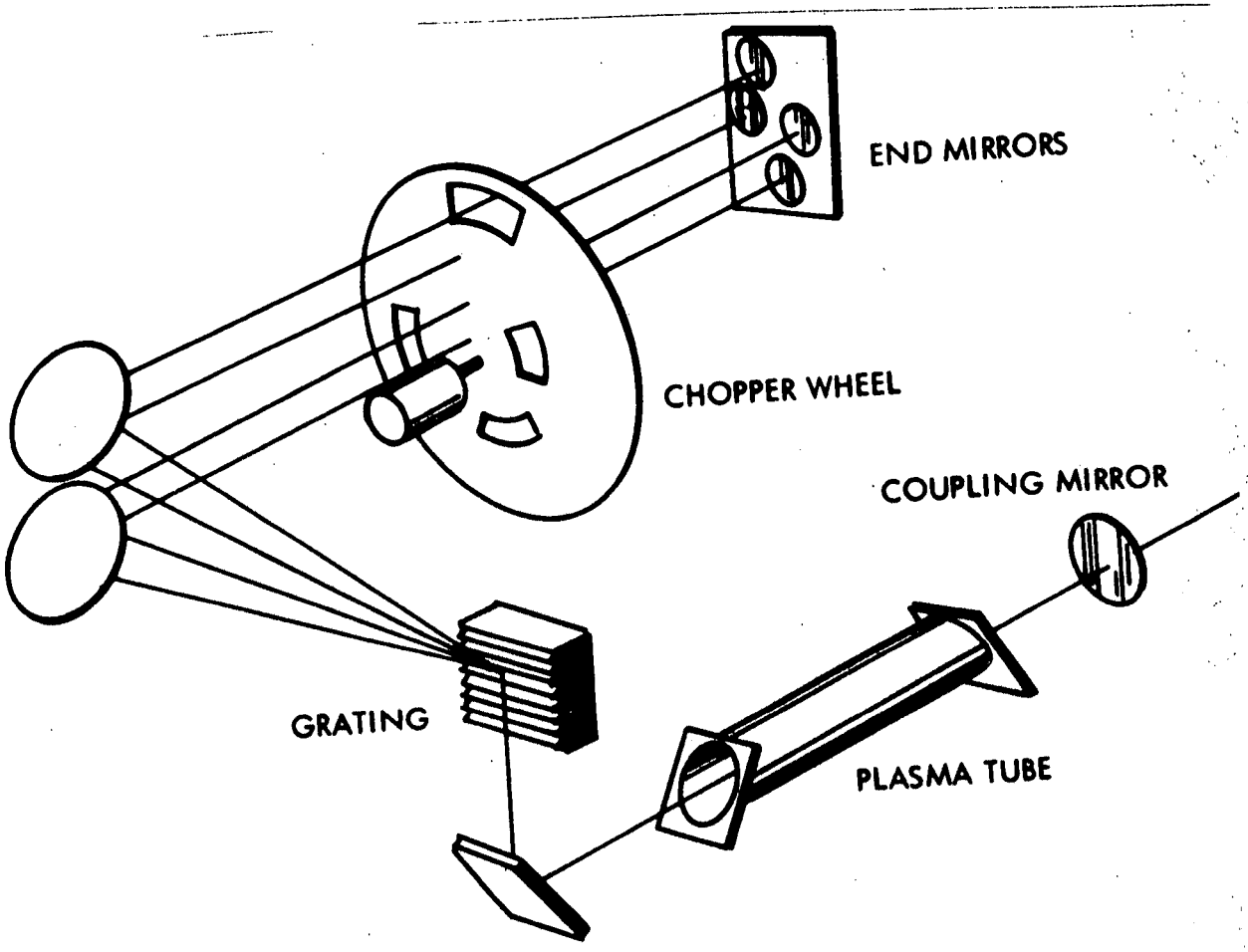

Figure 5. SPECTRALLY SCANNING LASER DESIGN CONCEPT

beamsplitter was removed, and another, significantly different, beamsplitter was installed to achieve acceptable performance. This beamsplitter was made from .020 Ge with a 42' (minute) wedge. It was oriented in the system so that the anti-reflection coated wedge surface was presented to the return signal. Backscatter of the transmitted beam from beam propagation optical elements was a continual problem. The focussing lens was operated off-axis to minimize this effect.

A new, digital processor-compatible preamp was designed for the thermistor bolometer detectors used in the system. The design incorporates variable signal attenuation capability, 60 db in nine steps. This feature is particularly useful when operating over the range of return signal experienced with varying weather conditions. Two preamps, one each for the (return) signal and reference detectors were built and installed in the system. Other modifications included relocation of the return signal bolometer-preamp to the position shown in Appendix A, Figure 33, an easily removable, three section plastic laser cover and screw jacks for leveling the laser mount.

BEAM STEERING OPTICS

Beam steering optics were incorporated in the system to permit rotation of the laser beam through 360° in azimuth and approximately ±10° in elevation. They consist of two 4 x 14 x 24 cm. flat mirrors, positioning fixtures and structure to support the fixtures on which the mirrors are mounted. A picture is shown in Appendix A, Figure 36. The lower mirror, at about 45° with respect to the horizontal laser beam, directs it up through the roof of the trailer housing the system to the other mirror, also about 45° and thence to the retroreflector and back. The mirrors are mounted on identical fixtures, and are adjustable about the 45° axis. Both are also adjustable about an axis perpendicular to the 45° axis, though this capability has been disabled on the upper unit. The upper mirror and fixture are

mounted on a 360° turntable with coarse and fine adjustment as well as slew capability.

Micrometer adjustments on the lower mirror are positioned to facilitate observing return signal level on either a nearby oscilloscope or the teletype printout. The upper mirror is shielded from the weather by a cupola atop the trailer whose design is such that manual positioning of the beam exit window is required. Sighting optics have been installed on the laser channel for visual location of distant retros. A mirror drops into the path of the laser beam near the focussing lens focal point for sighting purposes.

SECTION V

FIELD MEASUREMENTS

SITE DESCRIPTION

Under past EPA contracts ILAMS has been operated in rural and urban atmospheres at ranges, laser to retroreflector distances, approaching 5 kilometers (three miles). More recently it was employed in a four wavelength configuration to monitor ozone over a 0.67 kilometer range. Under this contract the system was changed to a six wavelength configuration using wavelengths selected and weights calculated for simultaneous monitoring of ozone, ammonia and ethylene. The system and trailer in which it has been installed were moved to the St. Louis area and operated there for a period of about two months. The system was located at Site 103 of the RAMS (Regional Air Monitoring System) network, across the Mississippi River in Illinois but actually only about 3 or 4 kilometers as the crow flies from the center of St. Louis.

The system, housed in a 2.4 x 4.8 meter (8 x 16 foot) mobile office-type trailer, was located in a fenced area, adjacent to the RAMS station and about 4 meters from Big Bend Road, a two lane concrete highway. Located just outside a trailer window was a portable ozone monitor with several feet of inlet tubing extending well above the trailer roof. The system was operated over several monitoring paths at this site. The first two were about 500 meters long. The last one, which was about the longest we could get at this site without considerable preparation, exceeded 900 meters. See Figure 6. Much of it was over the two lane concrete highway. The

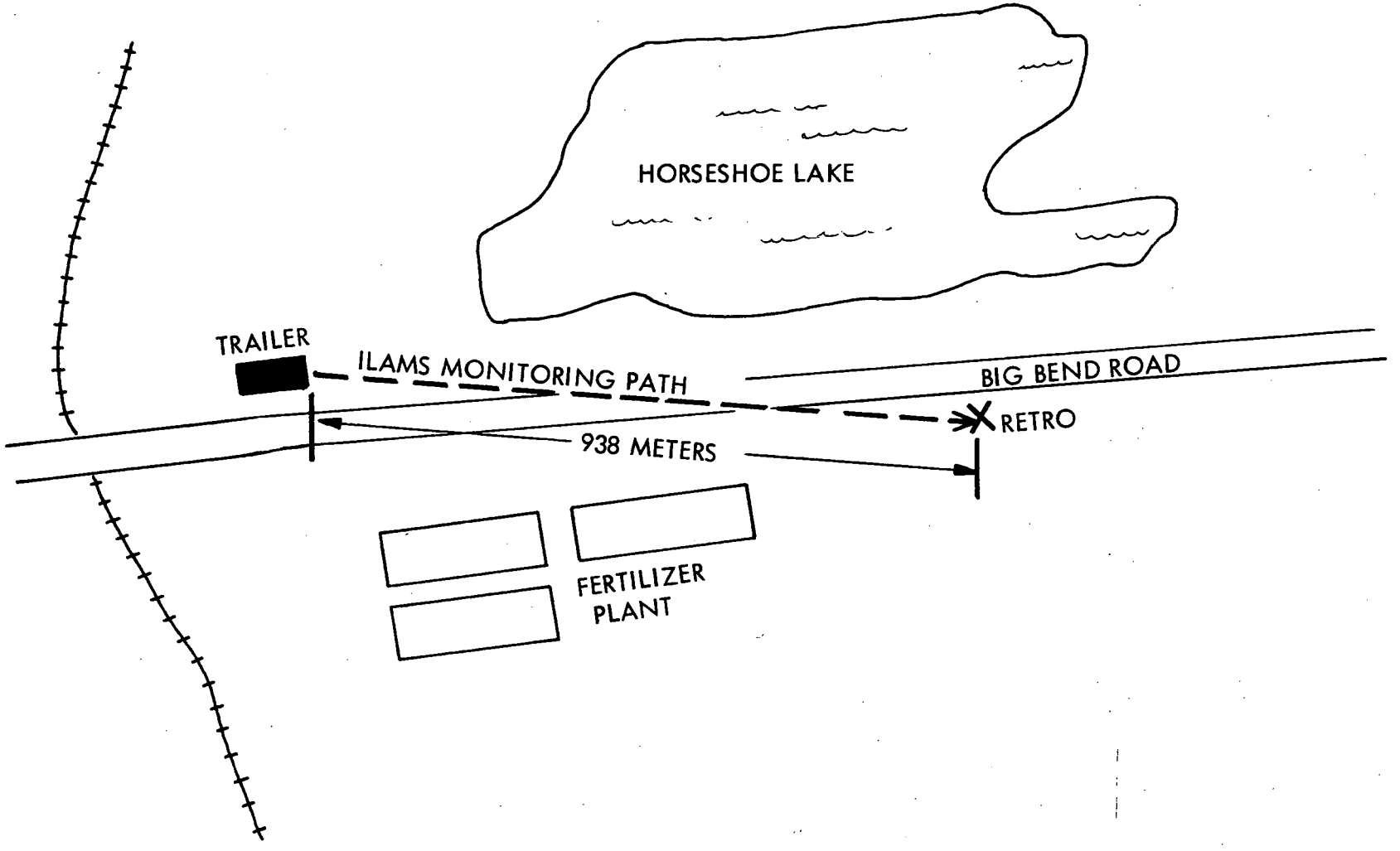

Figure 6. LAYOUT OF MONITORING PATH AT RAMS SITE 103

height of the laser beam (monitoring path) above ground ranged from about 1.0 to 3.5 meters. The highway proved to be a significant scintillation source. There was visible shimmer from it when looking down the path with binoculars on sunny days.

Across the highway and paralleling it toward the other (retro-reflector) end of the monitoring path was a long galvanized sheet steel structure 50 to 60 feet high housing a fertilizer plant. In the complex of buildings surrounding it was a large ammonia storage tank which appeared to serve as a distribution point to bulk ammonia users. The fertilizer plant was thought to be an ammonia source too, as well as the nearby stockyards. In addition, the plant was the source of dense pinkish-tan particulate emissions coming from a stack about as high as the main structure. After a period of such emissions, dust was everywhere. Settling on the long sloping roof of the main building, it gave a pinkish cast to the structure. Figures 7 and 8 are views from laser and retro ends of the monitoring path.

OPERATIONAL EXPERIENCE

Because early system performance was not in accordance with expectations, an extended period of experimentation and system adjustment followed setup and initial operations in St. Louis. As discussed in the Laser Modifications section, the beamsplitter was changed and the second pinhole removed, giving improved results based on cut and try experiments performed at the site. In the signal processor, the quantization level of the signal and reference channels was lowered to reduce quantization noise in low level signals. A processor function which set negative input samples to zero was disabled because it was introducing an intermittent positive bias to some signals. Such a condition might possibly occur when operating with a quarter second time constant under high scintillation but was not likely with the 32 second time constant used in St. Louis operations. The function substituted a zero when a negative return signal level occurred

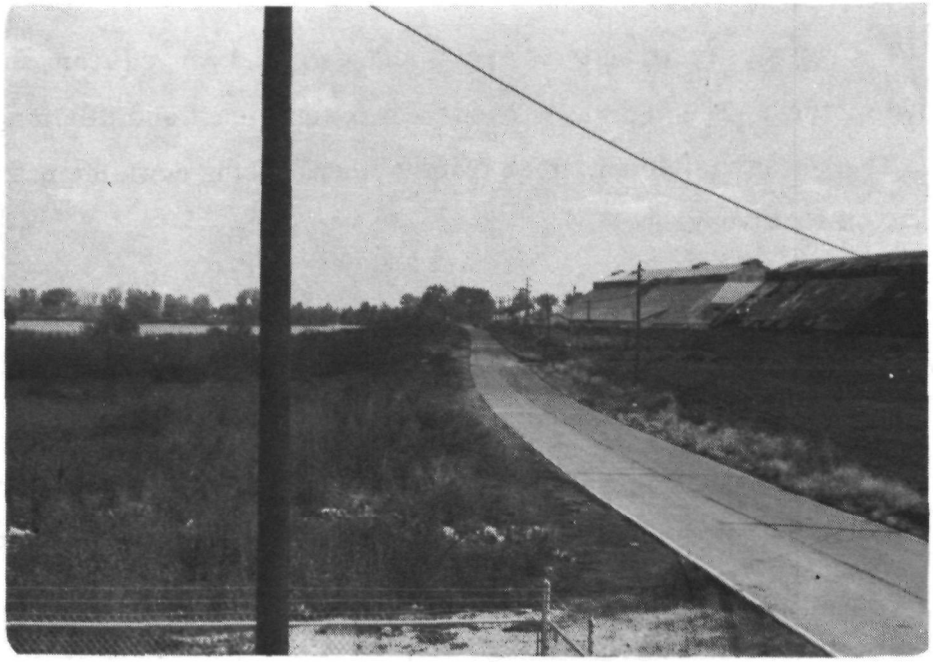

Figure 7. VIEW OF MONITORING PATH FROM LASER TO RETRO

Figure 8. VIEW OF MONITORING PATH FROM RETRO TO LASER

and this was thought to be biasing the data.

A "cat's eye" retroreflector (telescope with a plane mirror at its focal point) was used in the 1974 field tests. Prior to departing for St. Louis, the effect on system operation of a cube corner retro (three mutually orthogonal reflecting surfaces) was compared with that of a cat's eye. No significant difference in system performance was observed. Consequently, a 5" effective aperture cube corner was used initially in St. Louis (because of handling convenience) at ranges up to 800 meters. However, the reflecting surfaces corroded rapidly due to insufficient Si O overcoating and it became necessary to return to cat's eye operation.

Focussed vs defocussed beam experiments conducted during the course of the work showed a more stable return signal was achieved with the latter configuration on both transmit and receive beams. The reason for this was not clear. Defocussed operation was adopted for data taking. Operation with spatial filter pinhole sizes ranging from 0.25 to 0.91 millimeters (0.010 to 0.036 inches) indicated a 0.71 millimeter aperture as best for operation at the final operational range. Experience with beam steering optics produced estimates that once located, moving the laser beam to another retro would take less than five minutes and with some minor improvements 30 to 60 seconds. Time for initial retro location would also be reduced with these improvements.

There was evidence of trailer ambient temperature changes affecting system performance but attempts to isolate the cause were unsuccessful. An effort was made to keep ambient temperature as constant as possible with a system of thermometers and judicious operation of the trailer s air conditioners. Elements of the laser proved to be insensitive to blasts of hot air

from a hair dryer. The effects of changing temperature on the laser cavity are expected to be compensated for by the spatial filter. It has been suggested that the reference beam path could be the source of the problem, but this has not been investigated.

Line voltage variations and transients were a frequent problem at the monitoring site. A separate line was run from the power distribution point for the laser high voltage power supply to isolate it from other apparatus in the trailer. Transients were the cause of occasional computer stoppages. Some of the transients were associated with air conditioner on-off cycles. (Use of a ferro-resonant isolation transformer between the line and the computer is expected to solve this problem).

DATA

Early St. Louis data reflected the difficulties discussed above. Some indication of the nature of the problem can be seen in a comparison with similar data taken last fall. Figure 9 is a plot of O_3 count variation with time for 6 Sept 74 data. For the time period shown, each point on the plot is the average count for a one minute interval, 12 lines on the teletype printout. Count, or the number on the printout, is equivalent to a αCL (See Appendix B) and ozone concentration, 2.0 ppb/count for an 800 meter operating range. For comparison, Figure 10 shows 3 Dec 73 data plotted the same way. Its relative "smoothness" is evident.

Most of the path-point monitor comparison data taken in St. Louis related ILAMS output to the stationary point monitor outside the trailer window. However, on 3 Oct 74 some moving point monitor data was taken, i. e. the portable ozone monitor was walked along the 938 meter path. This data is listed in Table 5 and plotted in Figure 11. Figure 12 shows 3 Dec 73

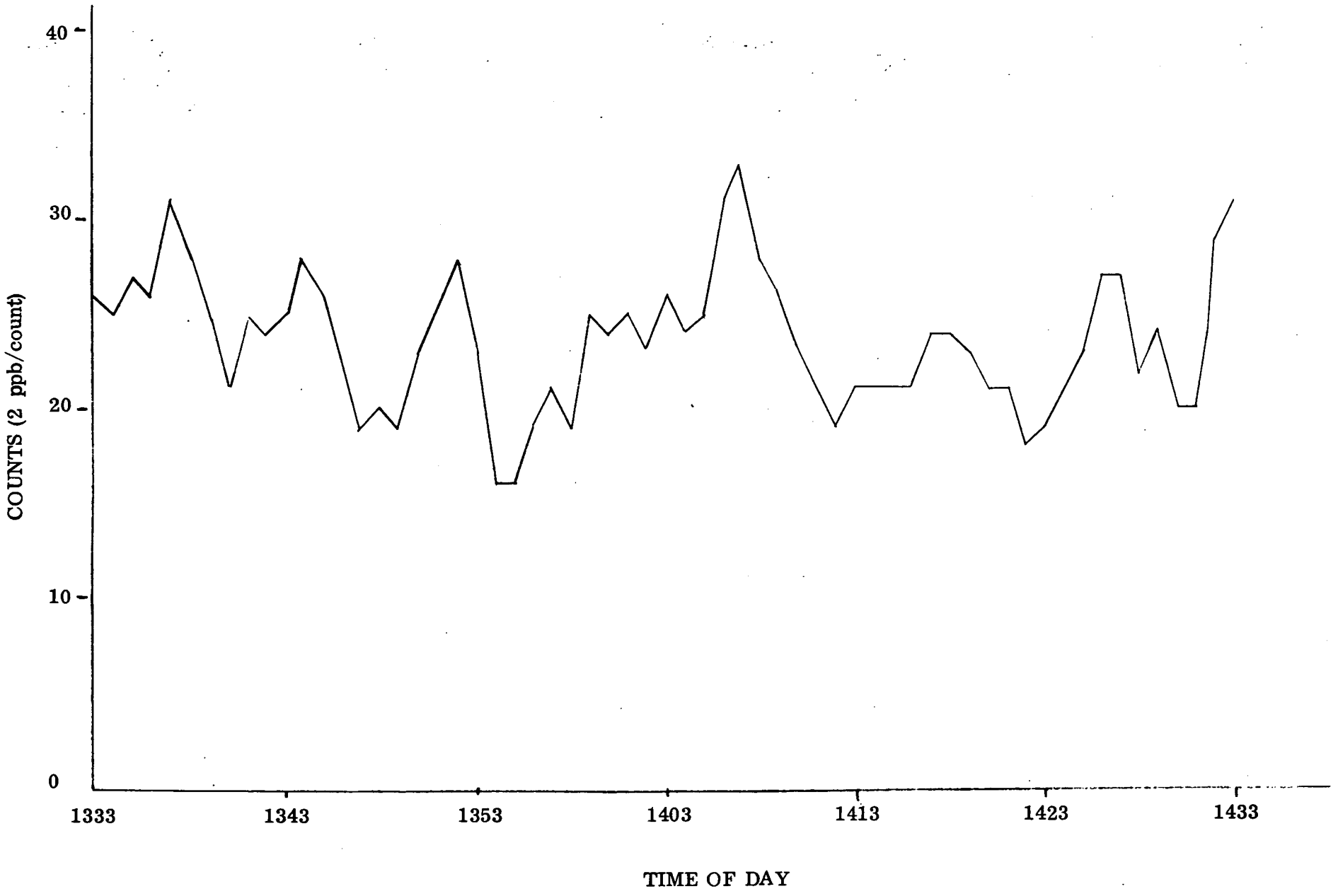

Figure 9 OZONE COUNT VARIATION WITH TIME - 6 Sep 1974

Figure 10 OZONE COUNT VARIATION WITH TIME - 3 Dec 1973

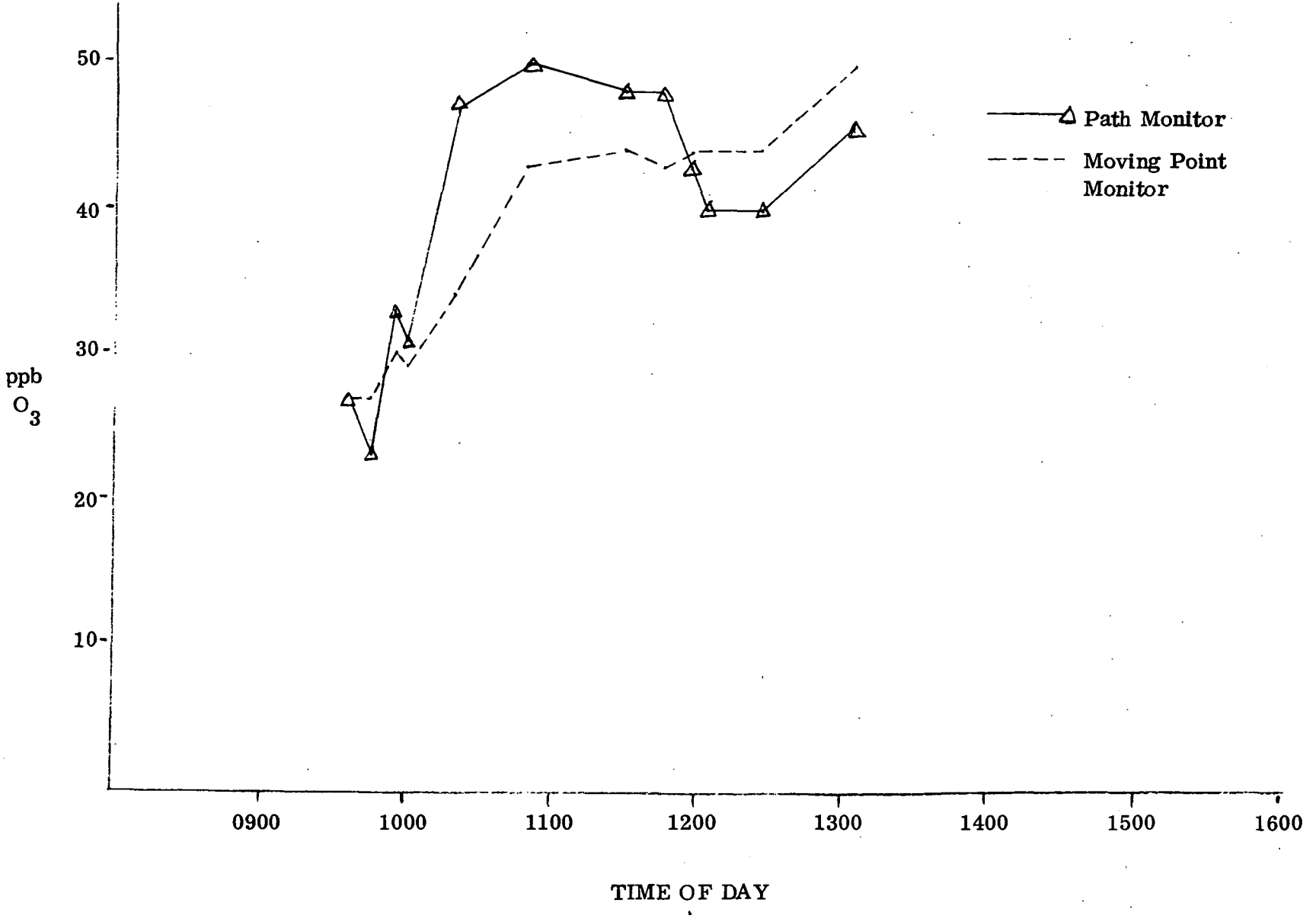

Figure 11 COMPARATIVE PATH/MOVING POINT MONITOR OZONE DATA - 3 Oct 1974

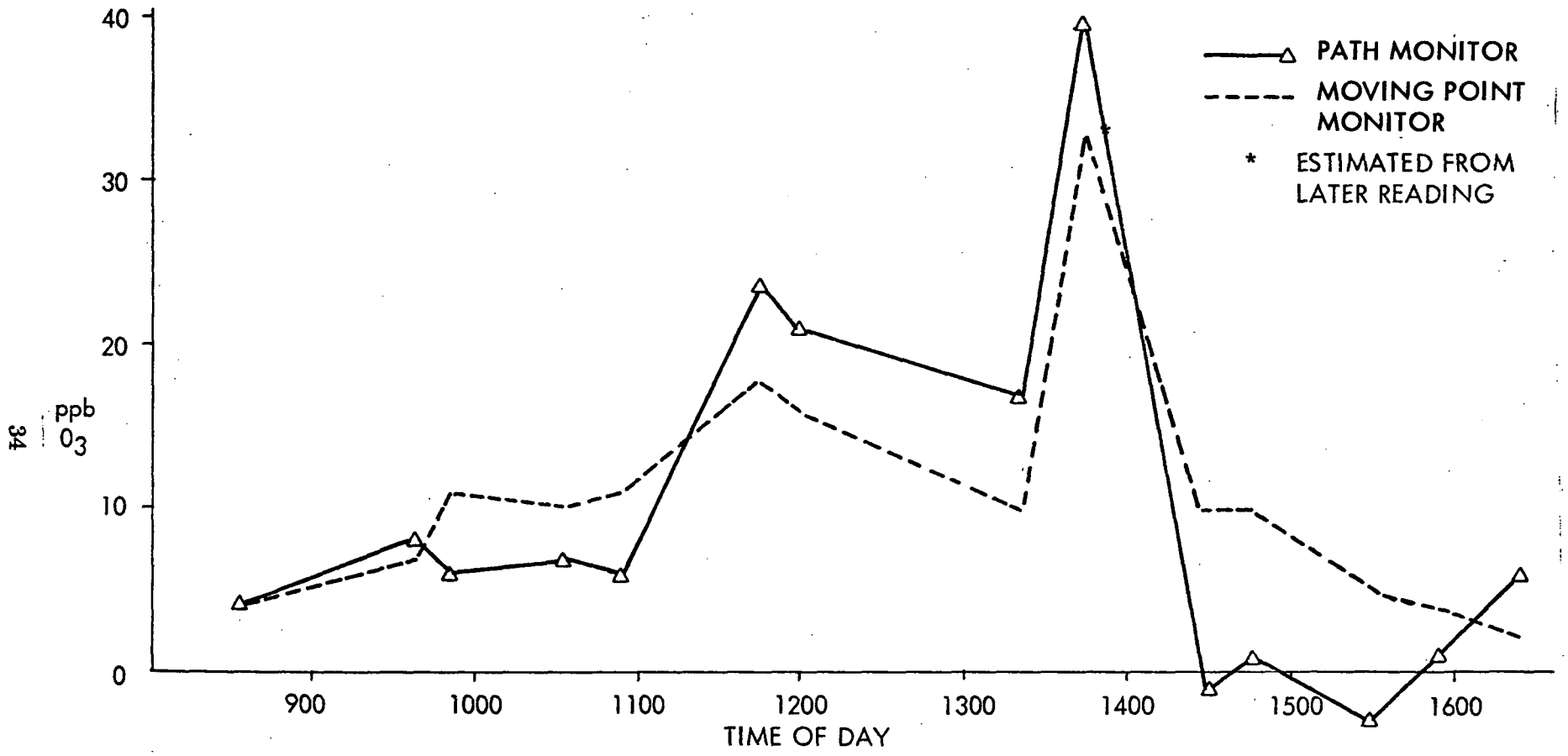

Figure 12. COMPARATIVE PATH/MOVING POINT MONITOR OZONE DATA - 3 Dec 1973

Table 5

3 Oct 1974

COMPARATIVE PATH/MOVING POINT MONITOR OZONE DATA SUMMARY

(ILAMS from Brush 2-Channel Recorder Chart)

	O_3 ppb	
Time	ILAMS	AID
0934	27*	27**
0945	23*	27*
0952	33*	30**
1000	31*	29**
1015-1029	47	34
1039-1055	50	43
1130	48*	44**
1145	48*	43**
1150	43*	44**
1200-1214	40	40
1217-1237	40	44
1303	46	50**

* one minute average

** Stationary

path/moving point monitor data for comparison. As Table 5 indicates, some stationary point monitor data is included in Figure 11. By this time in St. Louis what problems could be had been resolved and the comparison is favorable. Unfortunately, what looked like a good day of data-taking was interrupted by an area-wide power failure.

Other examples of data taken in the usual format are shown on the following pages, Figures 13 through 16. They were taken over the 938 meter path. The data, in the form of analog chart recorder traces, is for the two days 9 and 10 October 1974. For each day there is a comparison of ILAMS data and that of a portable chemiluminescent monitor, Analytical Instrument Development Inc. (AID) Model No. 560. Also, for each day there is a two channel chart recorder trace showing ILAMS ozone and ammonia concentration data side by side. Time on the path and point monitor traces runs from right to left. On the O_3/NH_3 traces, time runs from right to left too, beginning on the top, and continuing on the bottom chart.

The zero baselines on Figures 13 and 15 are at the bottom of the traces. On O_3/NH_3 data there is a separate scale grid for each trace, so the baseline or zero for the upper one is a little above the midpoint of the charts reproduced in Figures 14 and 16. Zero for the lower trace is a short distance above the bottom edge of the chart reproduction. The ammonia trace was near zero much of the time. Recorded operation typically began around 9:00 AM and continued into the evening, usually around 7:00 or 8:00 PM. Such was the case on these days. Both were bright sunny days with early morning haze.

Figure 13 shows comparative path-point monitor data for 9 October. Both traces reflect the diurnal rise and fall of ozone concentration. The practice was to "zero" ILAMS by adjusting its chart recorder trace to correspond in concentration value to the point monitor trace. This was done by introducing a fixed bias or offset in the fluctuating ILAMS output and then waiting to see if it produced the desired correspondence. The procedure was subject to error, particularly when the effect of a rising or falling ozone concentration was added to the short term fluctuations in the AID output. Consequently there is early morning evidence of system output adjustment in the ILAMS chart records and any error in duplicating the point monitor trace location remains in the path monitor trace as a constant offset throughout the day.

The midday discontinuity in the ILAMS trace of 9 October results, as best we can tell, from beam blockage when the system was left unattended during lunch time. An earlier beam blockage produced by a truck leaving the fertilizer plant produced the swing to full scale visible on the trace earlier in the day. The midday discontinuity required reloading of computer programs and system rezeroing. A software change to prevent this from happening has been designed and incorporated in a new program which awaits final debugging. Later in the day, the ILAMS trace exhibits some variability which is the result of deliberate changes in beam position on the retro to assess their effect on system performance. Also evident in the stationary AID trace are some local, short term dips in ozone concentration not seen by the path monitor. These dips generally correlated with the passing of cars and trucks. They were attributed to NO from vehicle engine exhaust combining with O_3 to reduce the local concentration. In Figure 14, the characteristics of the ILAMS ozone trace discussed above are repeated at a little higher chart speed. Also apparent is the lack of ammonia, consistent with the wind data we have

showing that it was blowing away from the point monitor and the system monitoring path to the fertilizer plant.

Figure 15 again shows the typical diurnal rise and fall of ozone on 10 October 1974. Because the concentration level approached 120 ppb, a 5x scale change for both monitors to keep the trace on the chart followed by a later return to the original scale is evident. The ILAMS trace again shows the early morning adjustment to the AID concentration level. Also a period in the morning is apparent (straight line) where the processor was turned off while the effect of some adjustments to the retroreflector secondary was assessed. As on the 9th there are local concentration dips in the point monitor trace which have been associated with NO from passing cars. The dips are greater in number and more pronounced, consistant with the shift in wind direction; i.e. from the road toward the monitor.

Of particular interest is system performance late in the day relative to that of the point monitor. Up to the point of scale change, path and point monitors were reading almost exactly the same. Not long after the scale change, which occurred around 6:10 PM, the point monitor ozone reading fell to essentially zero; whereas ILAMS did not. It held steady for awhile, then trended upward for reasons unknown. Such performance can possibly be attributed to unknown spectral interferences, inherent or atmosphere-induced optical drift in the system or a combination of both. A combination is the most likely, but in the absence of quantitative data it is impossible to determine the cause. However, conditions at the time invite speculation that a major contributor to ILAMS performance was an unknown spectral interference, which once identified, the system can discriminate against. First, the wind was blowing from the fertilizer plant, across the system's path. Effluent from the plant was visible in the beams of the lights

around it; it was dark by this time. Large ammonia concentrations, which tended to correlate with high particulate emissions, were evident in the system's HN_3 channel (see Figure 16). On the 12th of October, when the fertilizer plant was operating and the wind blowing from the monitoring path to the plant, ILAMS, operating as it was on the 10th, went down to zero like the AID monitor.

Figure 16 essentially duplicates the ILAMS ozone performance of Figure 15, but without the scale change, hence the periods of full scale saturation. As mentioned this was a day of high ammonia concentrations in the path. Early in the morning, when this was apparent from the trace, a 4x scale change was made to keep the trace on scale. The independence of O_3 and NH_3 response is evident in the Figure. While ILAMS performance was not compared with an ammonia monitoring instrument as it was for ozone, there is evidence to show that the system was indeed responding to ammonia. For example, plots of ammonia concentration signal level as indicated by different wavelength pairs correlate very well in time, and in amplitude, in relation to the ratio of their absorption coefficients. System performance and odor thresholds give a rough idea of concentration levels experienced. The indicated concentration change over the path was frequently 500 ppb or more when the system responded to ammonia. An ammonia smell was often evident at the fertilizer plant end of the monitoring path when the system was indicating NH_3 concentrations. A reported ammonia odor threshold of .037 mg/liter (about 50 ppm) suggests ILAMS was responding to a nine meter plume of 50 ppm ammonia when the indicated average concentration change over the path was 500 ppb.

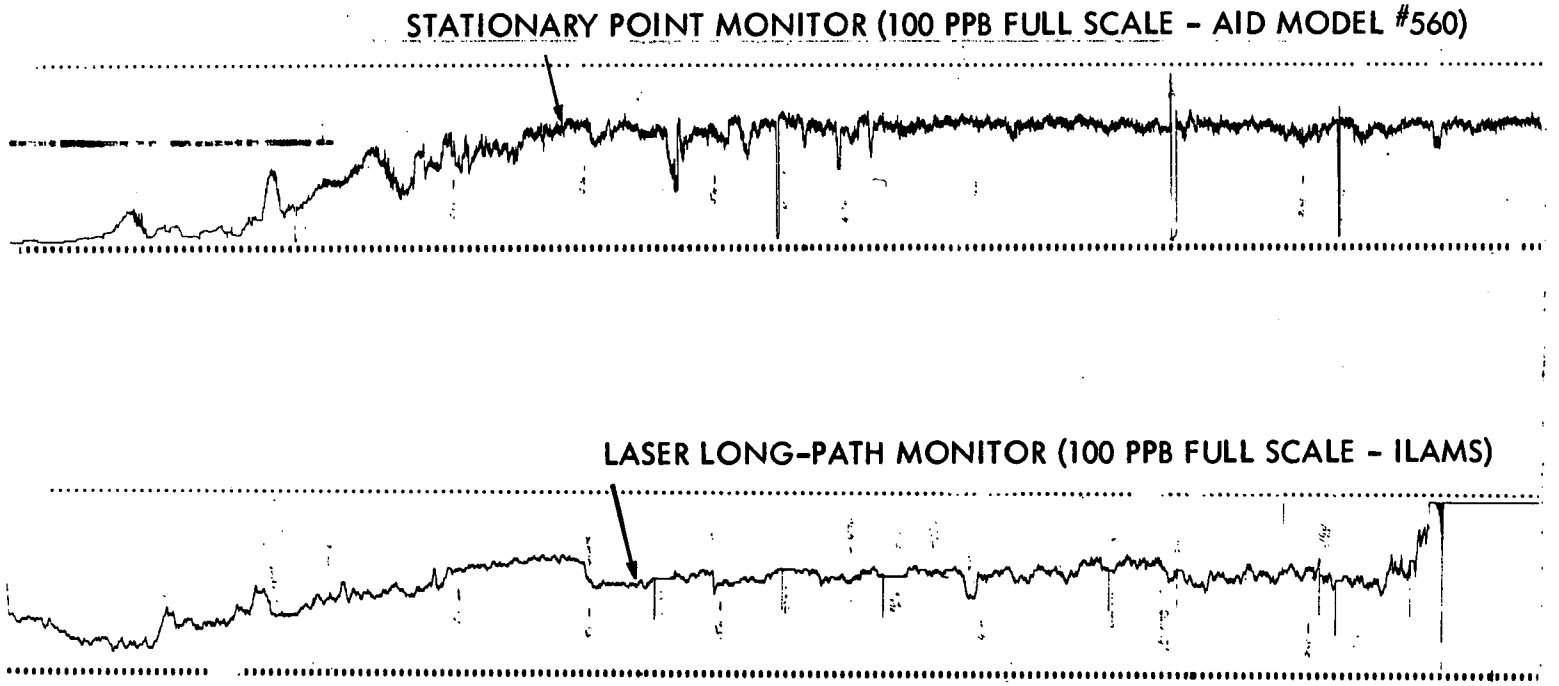

Figure 13. PATH & POINT MONITOR OZONE CONCENTRATIONS - 9 OCTOBER '74

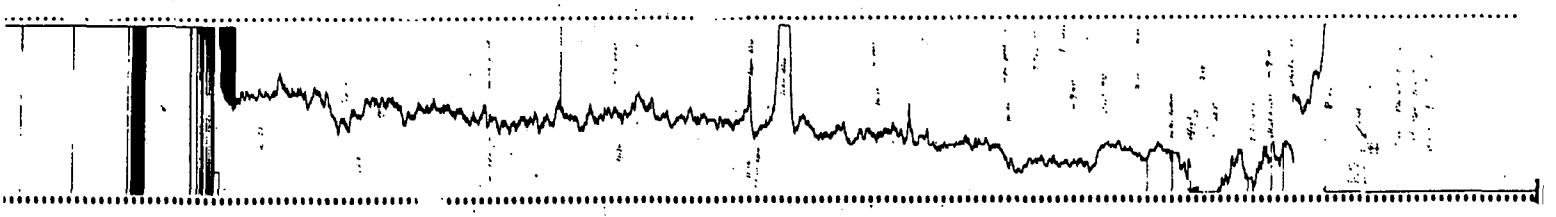

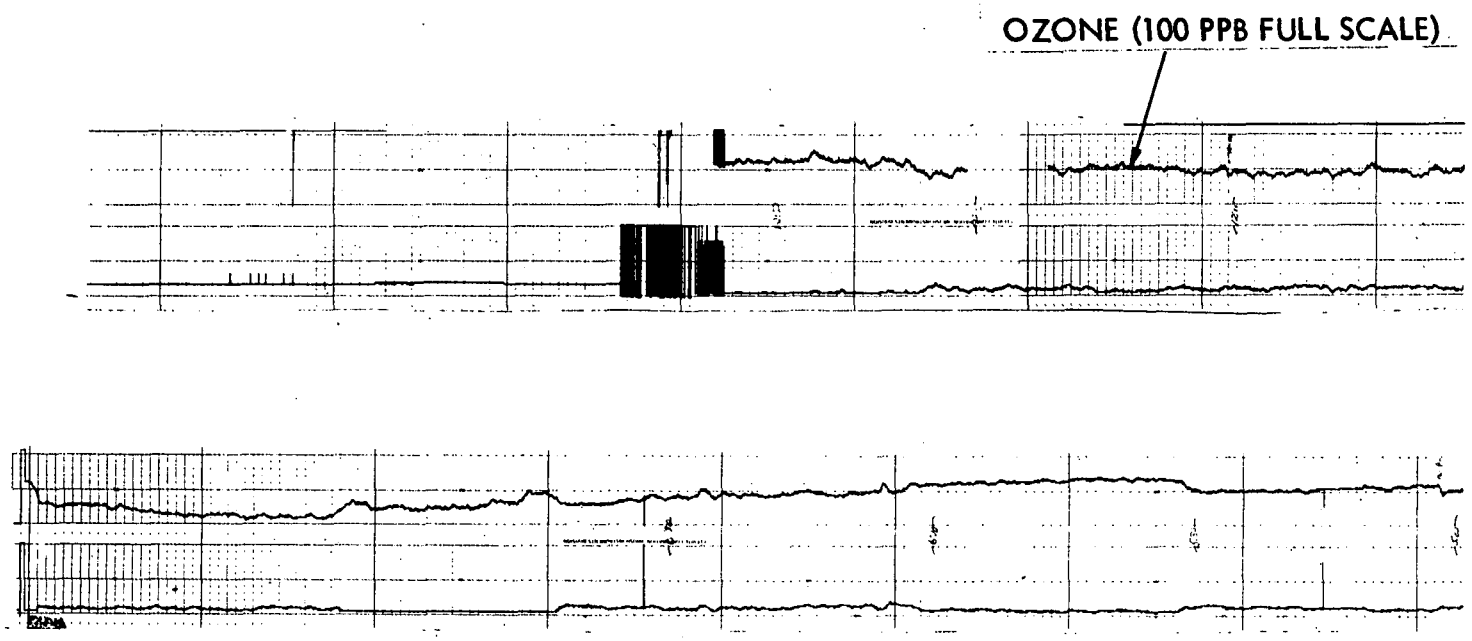

Figure 14. ILAMS OZONE AND AMMONIA CONCENTRATIONS - 9 OCTOBER '74

AMMONIA (UNCALIBRATED)

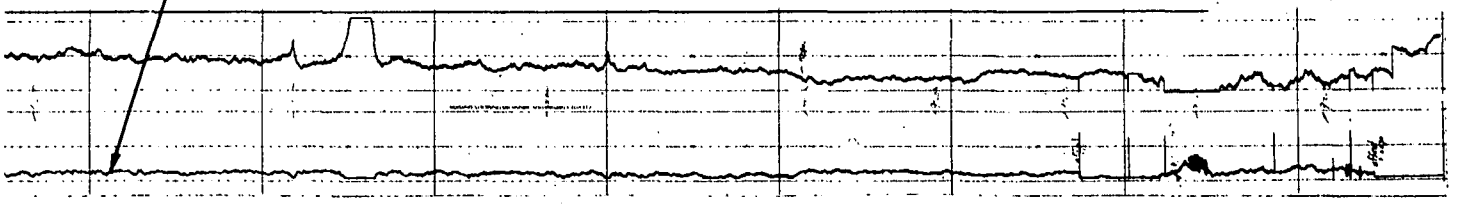

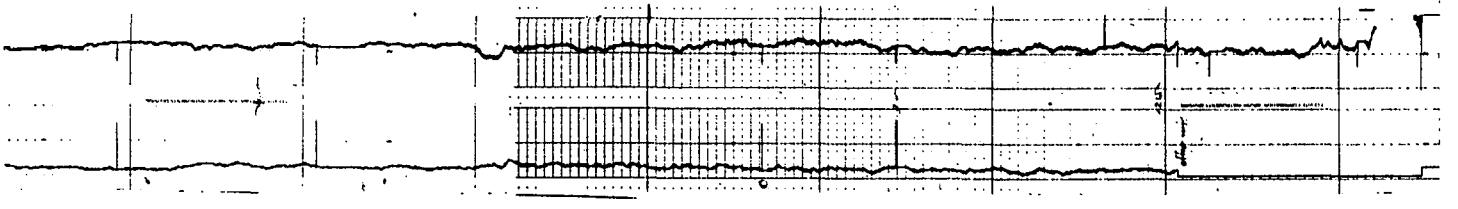

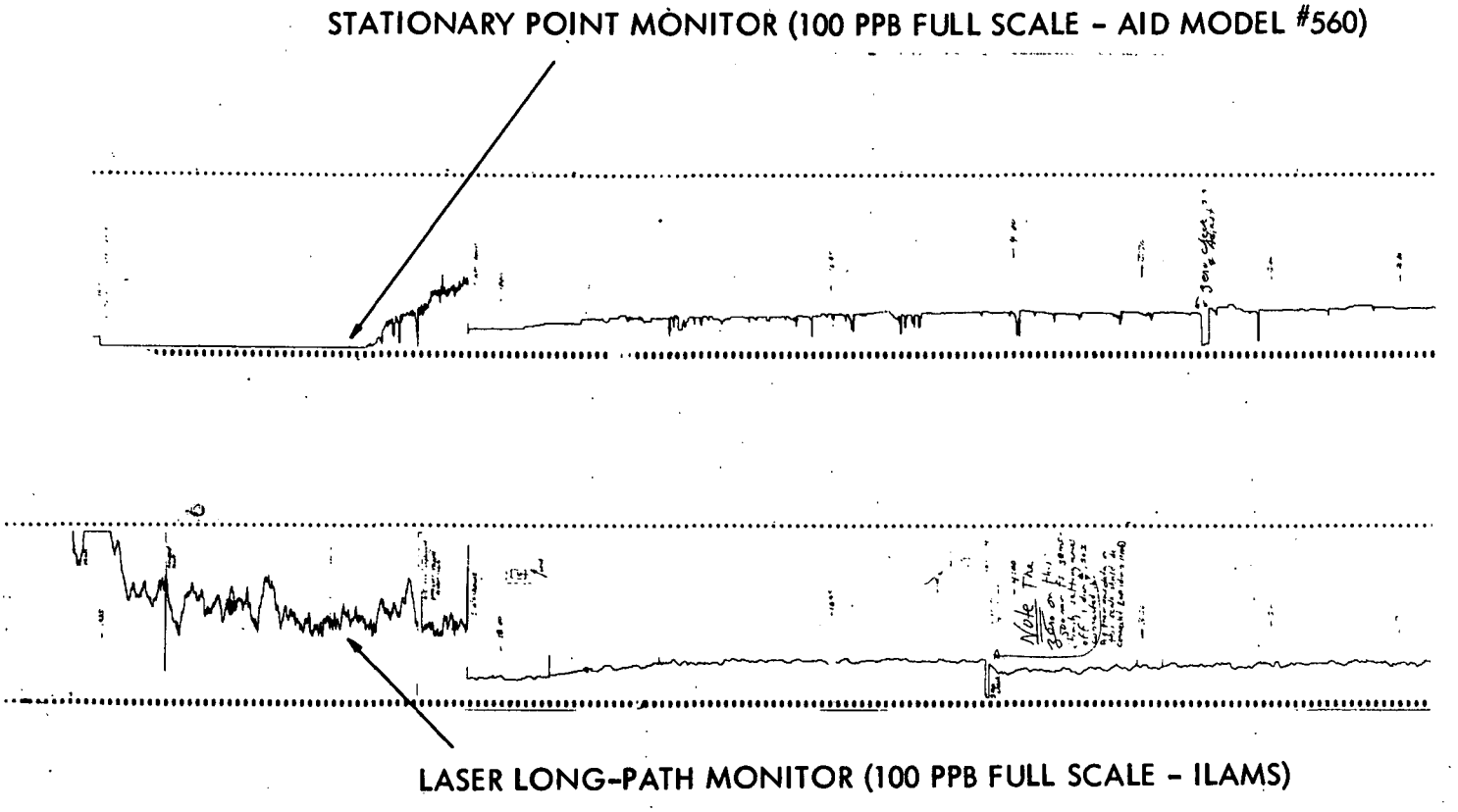

Figure 15. PATH & POINT MONITOR OZONE CONCENTRATIONS - 10 OCTOBER '74

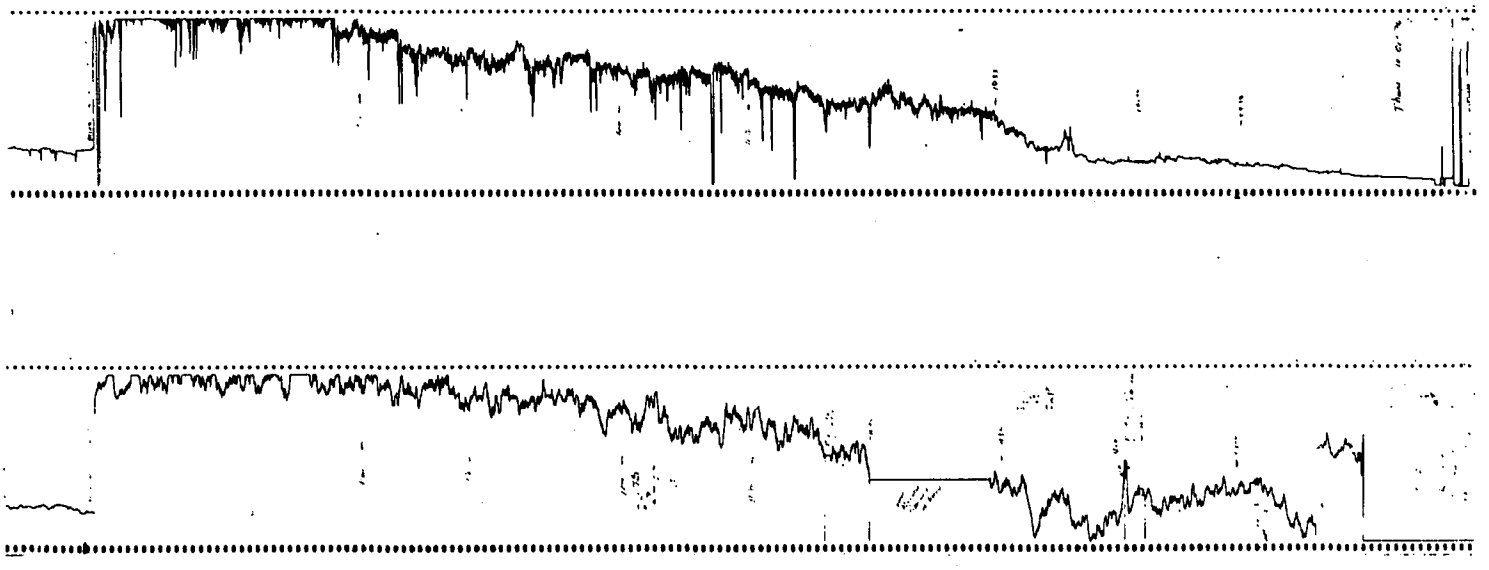

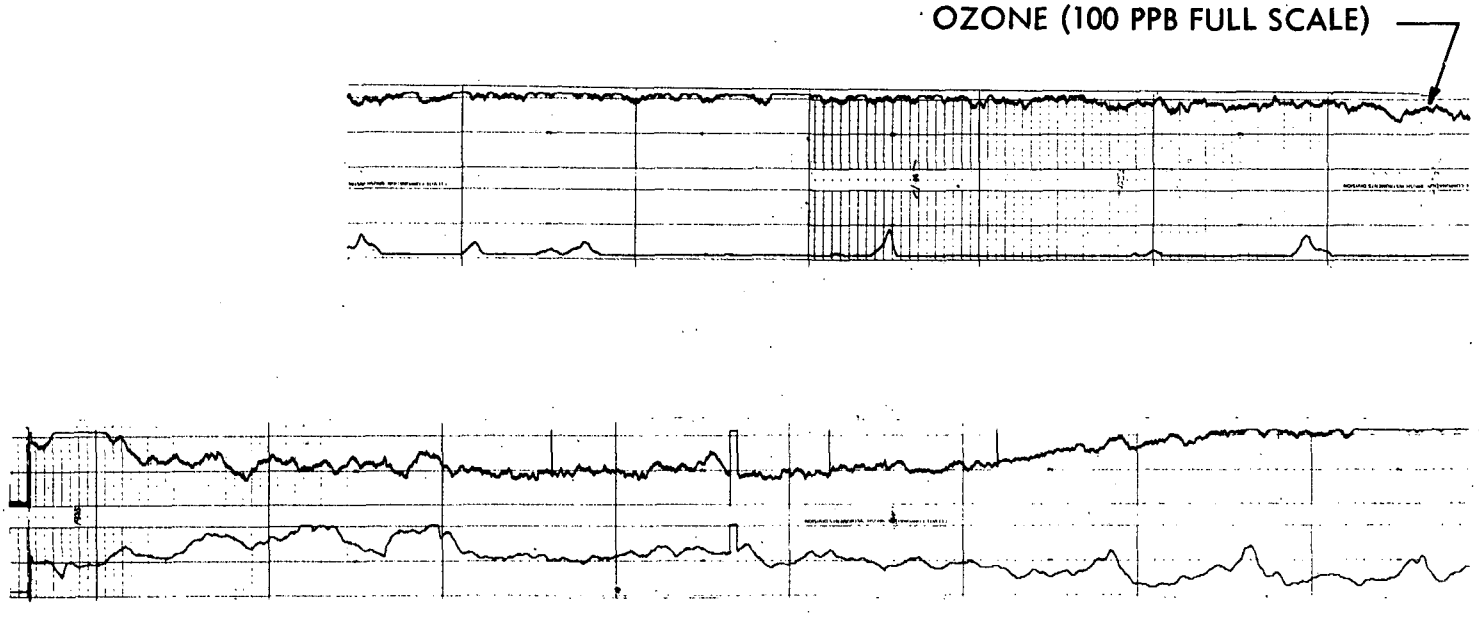

Figure 16. ILAMS OZONE AND AMMONIA CONCENTRATIONS - 10 OCTOBER '74

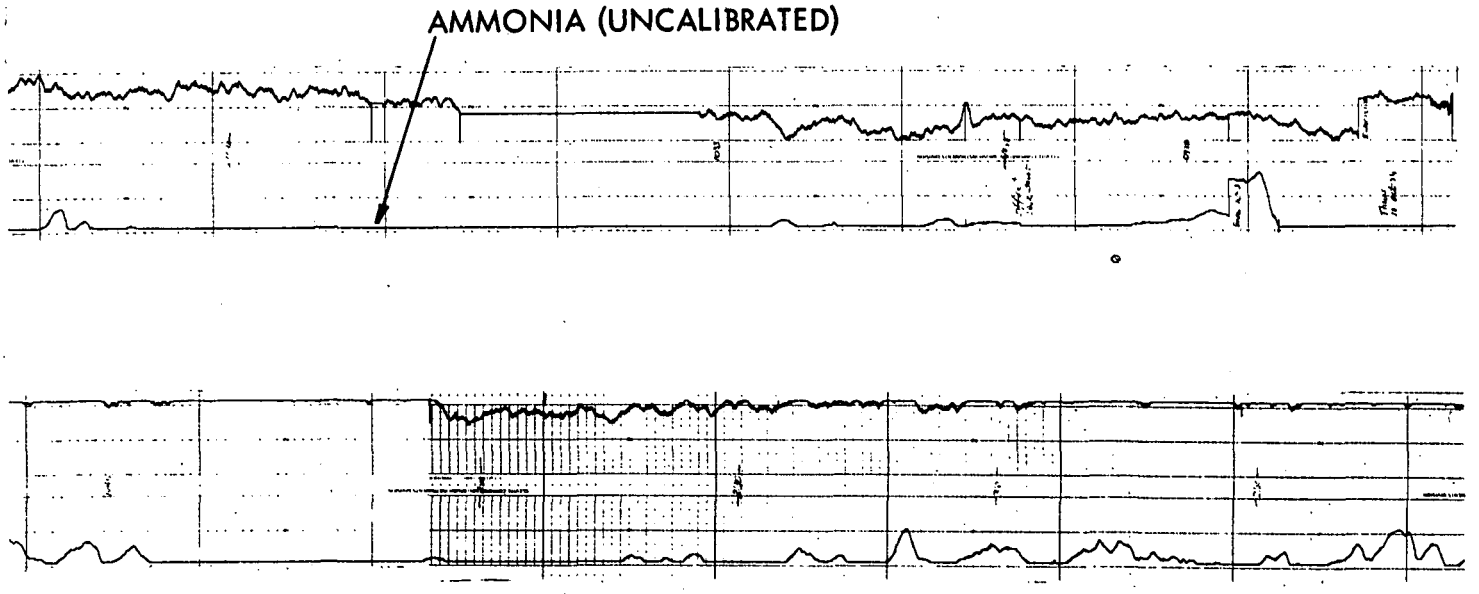
AMMONIA (UNCALIBRATED)

Section VI

DISCUSSION

Initial experimentation, analysis of the data obtained in St. Louis and reflection on the experience gained there has produced information which relates to the evaluation of the field measurement results and the direction of future activity to improve system performance.

SYSTEM ERROR SOURCES

With regard to optical problems in the system, the conclusions indicated by St. Louis data review are:

1. Non-uniformity in the power density of the laser beam over its cross-section (zoning) produces optical attenuation at the retro-reflector aperture and at the receiving mirror aperture. This optical attenuation is different at different laser wavelengths and hence upsets the absolute calibration of the system. The optical attenuation is changed by atmospheric turbulence and atmospheric looming causing drift errors in the measurement of gas concentrations. To achieve absolute calibration and bring the drift down to workable levels, this zoning must be eliminated.

2. Analysis of the data shows that the magnitude (but not the pattern) of the drift error between two wavelengths is roughly proportional to their difference in wavelength. Although this zoning-induced drift might be caused by spectrally dispersive optical elements in the transmitting and receiving optics, it

is more likely due to diffraction effects. According to Campillo et al,* the truncation of the laser beam at an aperture produces Fresnel zones at points remote from the aperture (depending on beam divergence). Moderate truncation results in large percentage amplitude variations.

Broadly speaking, there are a number of things, optical in nature, which could contribute to the spectral zoning that we feel is the major source of error in the system. (In discussing these effects, we visualize a multiwavelength transmitted laser beam, really a composite beam pattern, made up of the beams at each wavelength superimposed on each other at the collecting apertures in the system.) The conditions of concern are:

- Lack of far field concentricity of the beams at each wavelength.
- Beam size variation with wavelength.
- Non-uniformity in the power distribution across each wavelength's beam.
- Focussed vs. defocussed beam, return as well as transmit.
- Fresnel/Fraunhofer diffraction.
- Retro obscuration.
- Dispersion (refractive effects).
- Collecting aperture sizes.

There are many things which can be done to compensate or correct for these effects. In the beam propagation optics a spatial filter has been introduced to cleanup the laser beam, with the result that it made each wavelength's beam more uniform in power distribution across it and more concentric with respect to the others. However high resolution beam mapping has shown that the mirrors, lens and beamsplitter which follow it degrade the beam configuration produced by the spatial filter. Some of these elements can be eliminated or their degrading effects reduced. For example, an alternative to the beamsplitter was

* A. J. Campillo et al - "Fresnel Diffraction Effects"
Appl. Phys. Letters, Vol. 23, No. 2, 15 July 1973

tested early in the program as discussed later in this section in connection with beam mapping experiments. Backscatter from the focussing lens could be eliminated by replacing it with a reflecting element.

Diffraction effects are associated with the mode of operation, a focussed or defocussed beam. In Syracuse during the fall of 1973 we operated essentially focussed on both transmit and return. Fraunhofer diffraction effects occur in this mode. About the only relief from them, given good quality optics, is to operate in the central Airy disk of the diffraction pattern, overfilling optical elements. In St. Louis, focussed operation was too sensitive to misalignment. Defocussed operation on transmit proved to be more stable, and the return beam was slightly defocussed also. Fresnel diffraction effects are associated with defocussed operation and sharply defined "hard" apertures, like the exit of the collimator. To reduce Fresnel effects, the technique is to use smaller beam-to-aperture size ratios and soften or apodize limiting apertures.

Obscuration by the secondary mirror in the cat's eye retroreflector could be a significant effect in <u>non-focussed</u> operation but it has not been evaluated. If significant, a non-obscuring configuration like a cube corner (a cube corner and the cat s eye were found to be equivalent in <u>focussed</u> operation) or an off-axis parabola could be used. The use of larger collecting apertures to reduce optical effects such as atmosphere induced beam motion are a possibility, but have not seriously been considered because of cost.

Still another consideration is the reference beam path and the position of the spatial filter relative to it. Past practice has been to simulate, in the reference path, the return signal (far field) aperture-detector relationship. In current, defocussed operation, we still have a focussed operation simulation in the reference path. Also, changing the position of the spatial

filter appears to the reference detector as motion of the reference beam across the aperture in front of the reference detector. These effects need to be analyzed further and appropriate changes made. It has been suggested that the reference path is the source of at least some of the temperature sensitivity experienced.

It is clear that there are a number of optical configuration questions to be answered and that substantial effort is needed in this area. Treatment of the problems has so far been limited. It is expected that a thorough study of beam propagation optics will indicate changes, which, when implemented, will produce significant improvement in the performance of the system.

System zeroing was a source of error as noted earlier. In previous programs (References 1 and 4) the linearity of system response to ozone, ammonia and ethylene has been established for the concentration range of interest. For accurate concentration measurement with ILAMS it remains only to locate zero or some known concentration point on the response line, i.e., the linear plot of system response versus concentration. In St. Louis, system response for a known concentration (as indicated by the portable ozone monitor) was determined and the "zero" response extrapolated from that point knowing the ppb equivalent for one count on the printout.

An appealing alternative, which eliminates the need for another instrument to determine a point on the response line, is based on operating the system over a very short or negligible path length. Such a situation is easy to create by simply putting a retro, with appropriate attenuation, at or near the transmit optics. Over such a short path, pollutant gas concentrations would be essentially zero, and the system response over the abbreviated path would be equivalent to zero concentration. However, there is an important condition

to this approach. The multi-wavelength laser beam pattern and its relation to the retro (overfill, underfill, etc.) must be the same over the short and long path. The resolution of system optical problems should make it possible to at least satisfactorily approximate this condition.

Though not as extensively treated here or in the course of this work, there are other sources of error, potentially significant contributors, which also need to be examined and their error contribution determined. Among them are:

1. Electronic (thermal) noise
2. Quantization noise and sampling error of the signal and reference channels which are enhanced by the large range in laser power levels
3. Quantization error in the numerical weighting functions which results in poorer rejection of spectral interferences
4. Cross talk error caused by the high and low frequency response of the preamplifiers and laser signal power amplitude fluctuations
5. Scintillation noise falling within the information band width of the system
6. Spectral absorption and scattered sources in the atmosphere about which we have incomplete or incorrect information, or that are so large that they exceed the dynamic range of the system

ALTERNATIVE WEIGHTING STRATEGIES

It has been stated that St. Louis data review has revealed the presence of drift error associated with the spacing between wavelengths. While it appears that this error is caused by optics-related effects, it has also been determined that a change in weighting strategy is useful in reducing the wavelength separation dependent component of the drift error. Several

strategies have been tested on some of the data from St. Louis with these results:

a) Choosing two wavelengths close together to measure a particular target gas produces a significant improvement in drift

b) Using six wavelengths with weights selected to distinguish between correlated and uncorrelated optical noise works measurably better.

However, neither of these two approaches does a totally satisfactory job. It should be the objective of further analysis to gather additional evidence of alternative strategy effects. These alternative strategies can then be considered in the light of optical problem-solving results. It is a relatively simple matter to introduce and evaluate promising strategies in the data-taking during subsequent field measurements.

These observations about wavelength strategies have been derived from data taken on 11 Oct 74, a day when there was significant drift or random fluctuation in the ozone output record that was unrelated to the ozone levels as recorded by the AID point monitor. On that day some effluent was observed to be coming from the fertilizer plant. The weights indicated in Table 6 were applied to the teletype printout of αCL (the Beer's Law exponent - see Appendix B) at each wavelength using a hand calculator. By plotting these weighted outputs one can isolate the effects of both the effluent from the fertilizer plant and the drift error related to wavelength spacing. Curves generated in this way using the weights of Table 6 follow as Figures 17 through 22. The vertical scale of these plots is in arbitrary units; the horizontal is time of day. Based on the absorption coefficients listed in Table 2 the responses to each of those weights is given in Table 7.

TABLE 6

WEIGHTS CORRESPONDING TO EACH OF THE CURVES CALCULATED AND PLOTTED

CURVE NUMBER	WAVELENGTHS					
	1 9.25	2 9.29	3 9.50	4 10.53	5 10.63	6 10.70
1	-.5655	-.0527	+1	+.0388	-.9946	+.5741
2	0	0	0	0	-1	+1
3	-1	+1	0	0	0	0
4a	-1	0	+1	0	0	0
4b	-.9805	-.0195	+1	0	0	0
5	1	0	0	0	-1	0
6	-.95	-.05	1	+.0107	-.5292	+.5185

Table 7

RESPONSE TO EACH OF THE WEIGHTS SHOWN IN TABLE 6

((CROSS-RESPONSES))

	CURVE NUMBER						
	1	2	3	4a	4b	5	6
H_2O	-3.8×10^{-5}	0	0	0	0	-1×10^{-4}	0
CO_2	5.7×10^{-5}	-8×10^{-4}	5×10^{-4}	0	-10^{-5}	-1.4×10^{-3}	4.38×10^{-4}
C_2H_4	3.4×10^{-4}	-0.47	0.1	-.04	-.043	1.92	2.05×10^{-4}
O_3	12.7	0	0	12.7	12.7	0	12.7
NH_3	3.7×10^{-4}	0.73	12.64	0.246	-4×10^{-4}	-0.066	1.9×10^{-5}

11 OCTOBER 1974

9.25, 9.29, 9.50, 10.53, 10.63, 10.70 MICRONS

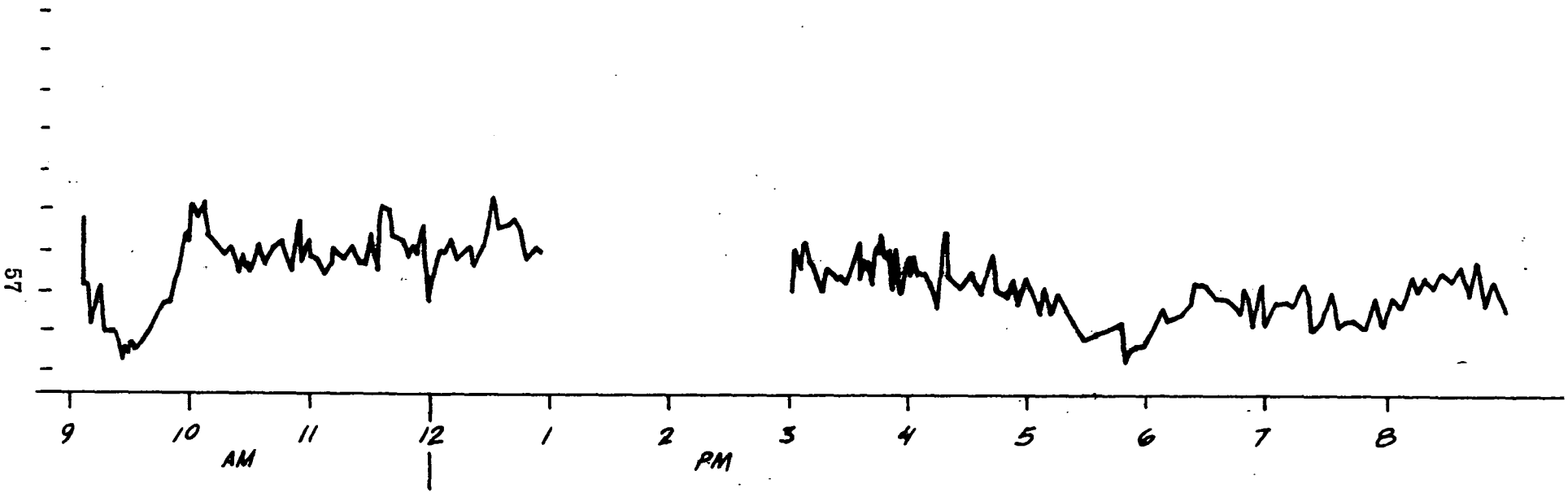

Figure 17. ST. LOUIS SIX WAVELENGTH OZONE

11 OCTOBER 1974

10.63, 10.70 MICRONS

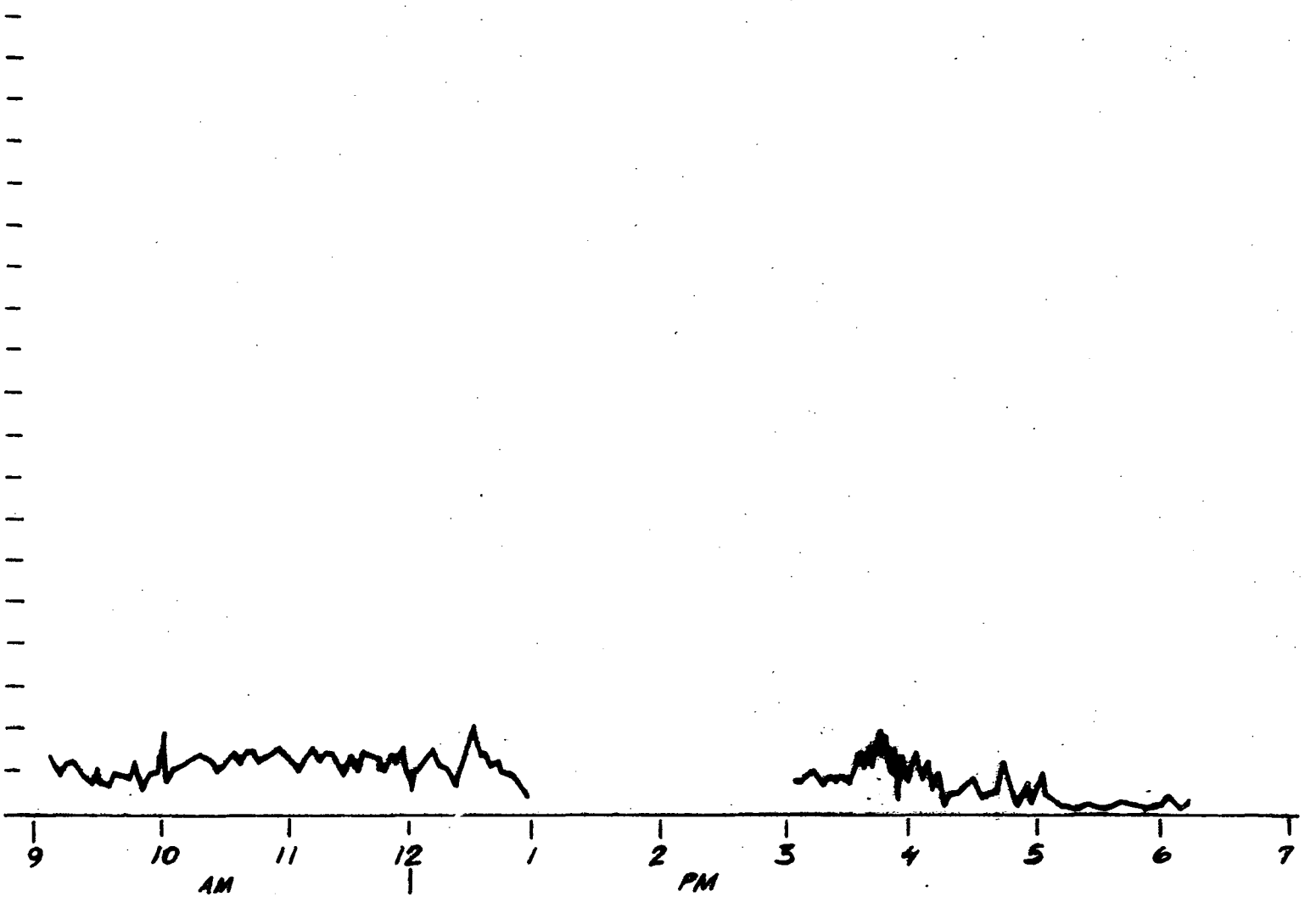

Figure 18. TWO CLOSELY SPACED WAVELENGTHS

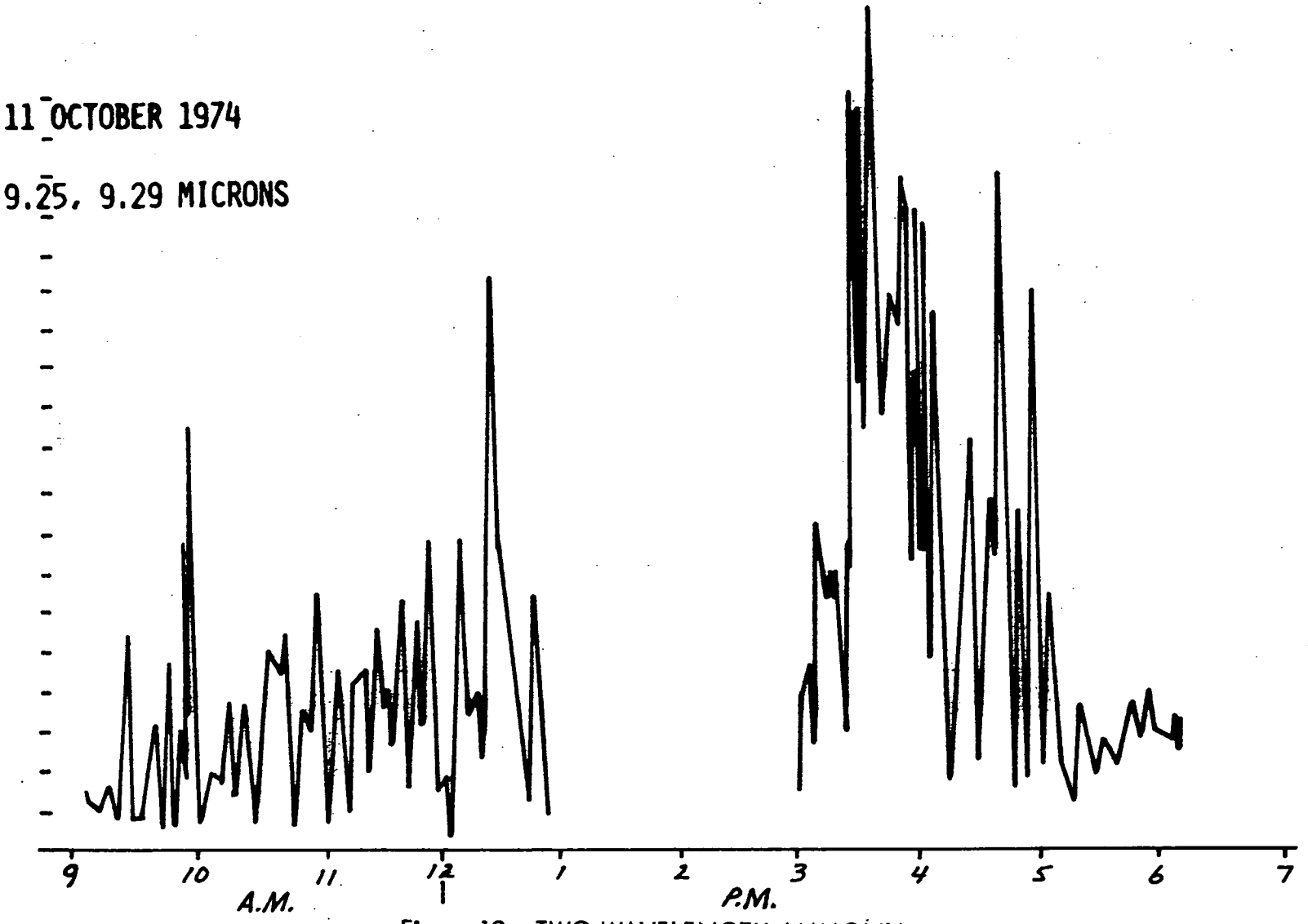

Figure 19. TWO WAVELENGTH AMMONIA

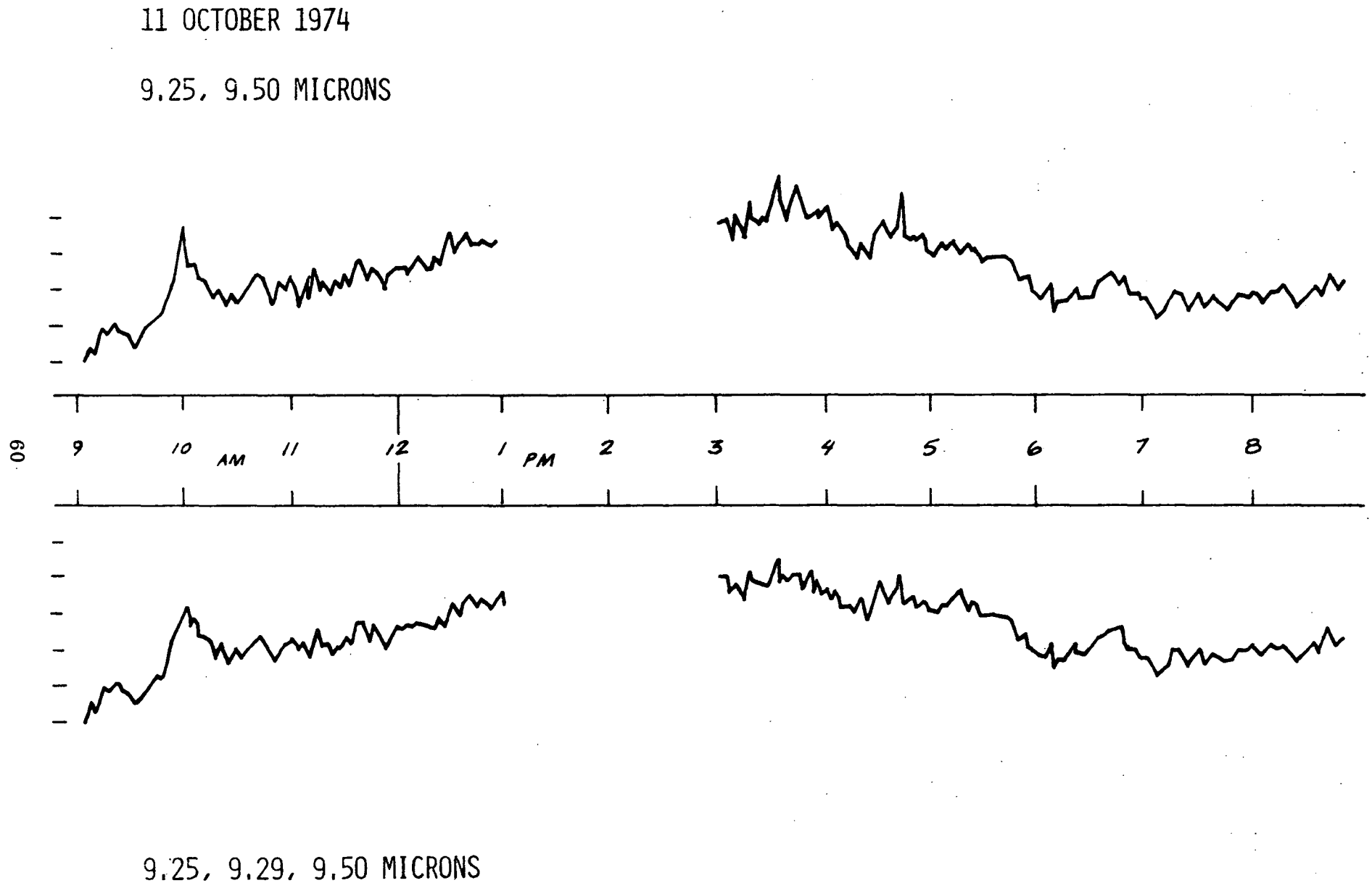

Figure 20. TWO AND THREE WAVELENGTH OZONE

11 OCTOBER 1974

9.25, 10.63 MICRONS

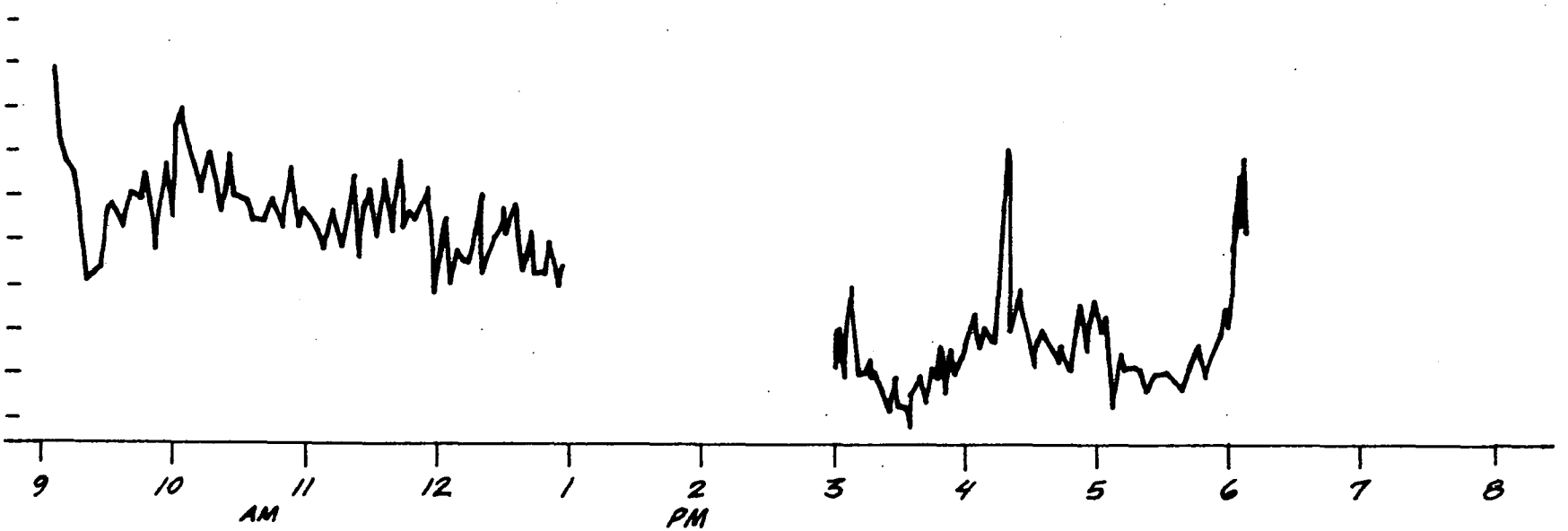

Figure 21. TWO WIDELY SPACED WAVELENGTHS

11 OCTOBER 1974

9.25, 9.29, 9.50, 10.53, 10.63, 10.70 MICRONS

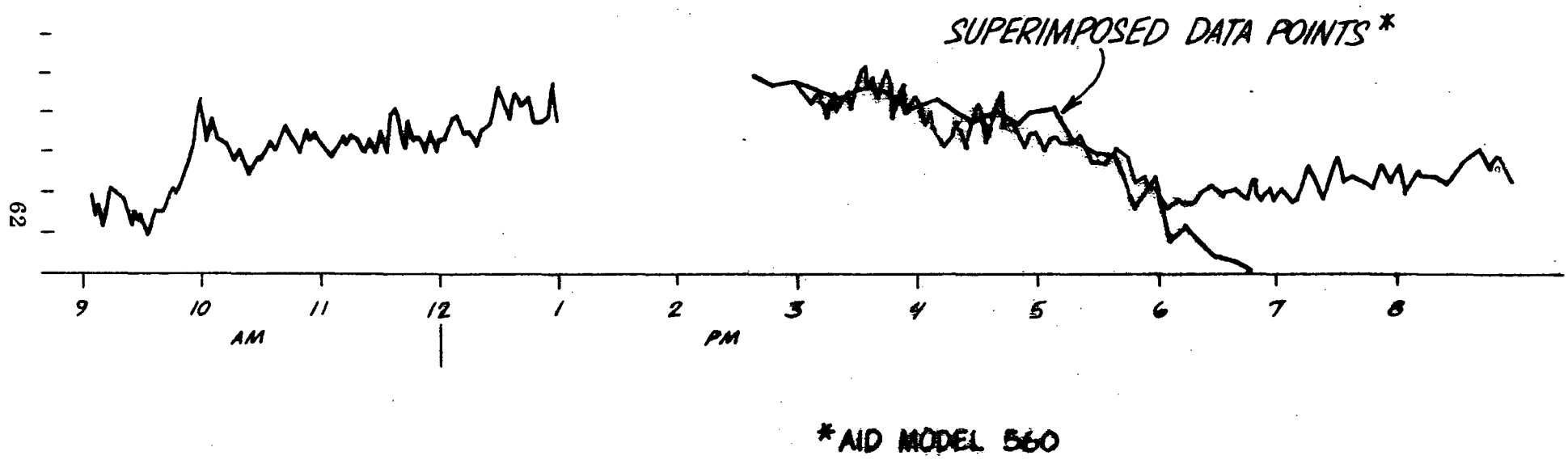

Figure 22. IMPROVED SIX WAVELENGTH OZONE

Figure 17 is a plot of the output weighted for ozone as a target and ethylene, ammonia, carbon diozide, water vapor and neutral attenuation as interferences. This is the same curve as was recorded on the chart recorder at St. Louis as the ozone output. The cross responses to this weight have a non-zero value because the covariance method was used to calculate the weights and system noise was considered along with the known spectral interferences.

Figure 18 was the first attempt to see if two closely-spaced wavelengths would exhibit very little drift. This plot showed larger fluctuation than expected, so the presence of ammonia effects was examined.

Figure 19 compares two closely-spaced wavelengths one of which is a strong ammonia line. This plot showed widely fluctuating ammonia concentrations with a maximum average concentration of 800 ppb. A comparison of Figures 18 and 19 showed that the two plots are an excellent match except for scale and that the ratio of scales is the same as the ratio of the expected responses to ammonia (see Table 7). This is good evidence that ammonia was the major spectral interferent in the effluent from the fertilizer plant.

Figure 20a is a two-wavelength system which responds strongly to ozone and only slightly to ammonia. This plot is considerably smoother than the plot of Figure 17 and tracks the AID data as closely as could be expected, except at the beginning and end of the day. This discrepancy was as bad as 40 ppb at one point after 7:00 pm.

Figure 20b is a closely spaced three-wavelength system designed to respond to ozone, and not respond at all to ammonia. This plot shows a further reduction in the ammonia response and no noticeable change in the errors at the beginning and the end of the day. There are three possible explanations for the presence of an ammonia pattern on this trace: 1) The

ammonia absorption coefficients used to calculate the weights are wrong, 2) Another spectrally interfering gas was mixed with the ammonia, or 3) The very large concentrations recorded for ammonia using a 32-second system response time are really the average of much larger, short-time-average concentrations moving in and out of the path producing at times complete extinction of the signal at λ_2. The system in attempting to quantize the residual noise produced some error.

Figure 21 compares two wavelengths that are widely spaced yet do not respond strongly to either ammonia or ozone in order to further assess the effects of wavelength spacing. The curve shows large drift compared to either Figure 18 or Figure 20, that is, large fluctuations in the amplitude that may or may not be due to fluctuations in the concentration of some gas or spectrally interfering material in the path. At times, at the beginning and end of the day when the drift on Figures 18 and 20 is obvious, the fluctuation on Figure 21 is correspondingly larger.

Figure 22 is the result of applying a weight that is designed to discriminate against the effects of wavelength spacing as well as produce low responses to all the spectral interferences. The cross responses are shown in Table 7. Besides having the insensitivity to the spectral interferences, this plot appears to track the AID data somewhat better than Figures 20a and 20b. However, the morning and evening drift is still apparent. Note that any weight that discriminates perfectly against both water vapor and neutral attenuation also discriminates against any random drift of the ten micron group of wavelengths with respect to the nine micron group. The weights used for Figure 18 had an adequate cross response for water vapor, but not for the random drift in return signal at widely spaced wavelengths.

The covariance technique for computing the optical weights did consider optical noise as an interfering source, but did not consider the fact

that the noise would be highly correlated between wavelengths that are closely spaced. A more judicious selection of weights would have resulted in a large improvement in the chart data taken in St. Louis. It appears that the weights used for Figure 22 are the best set in terms of what is known now.

HIGH RESOLUTION BEAM MAPPING AND OTHER EXPERIMENTS

To examine the effects of elements in the beam propagation optical system a number of one-dimensional plots were made of the laser beam intensity measured across the transmitting aperture of the system. In each case a horizontal scan was made across the center of the 4.8-inch circular aperture of the collimator with a 0.3 mm by 0.3 mm thermistor bolometer detector. The measured detector output voltage was read directly from an oscilloscope presentation of the bolometer output. The vertical scale is relative intensity. The significant feature of these curves is the variation in intensity with horizontal position which is a measure of the partitioning of power distribution across the axis. It is this partitioning or zoning that the spatial filtering is designed to remove.

Figure 23 illustrates the effect on a single wavelength of a pinhole type of spatial filter. The curves show the output beam from the laser with the beamsplitter removed (fig. 33) and with no intra-cavity mode stop (iris stop, fig. 33) in the laser in order to emphasize the benefits of spatial filtering. The optical configuration for this experiment is shown in Figure 24. Because the output beam goes more directly into the beam expander, the beam is smaller at the focussing lens and at the output than is the case when operating the laser in the ILAMS system.

The filter in this case was inserted at the focal point of the beam expanding collimator so that the only optical elements following it were the 45° mirror and the off-axis parabola of the beam expander. The spatial filter

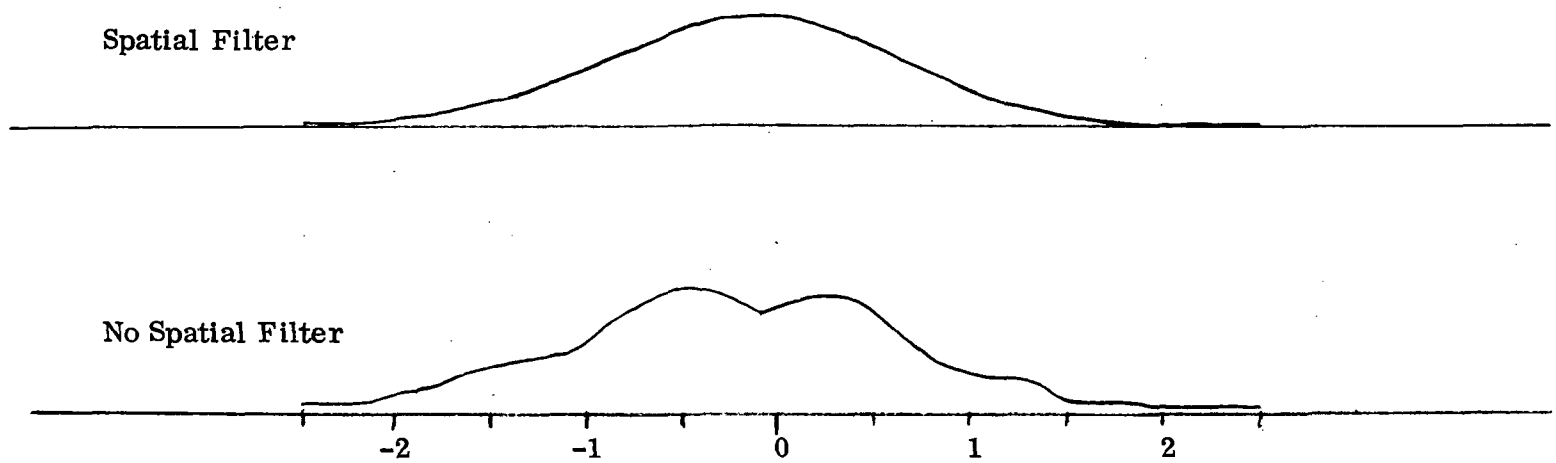

Figure 23 SPATIAL FILTER EFFECT ON ONE DIMENSIONAL INTENSITY DISTRIBUTION

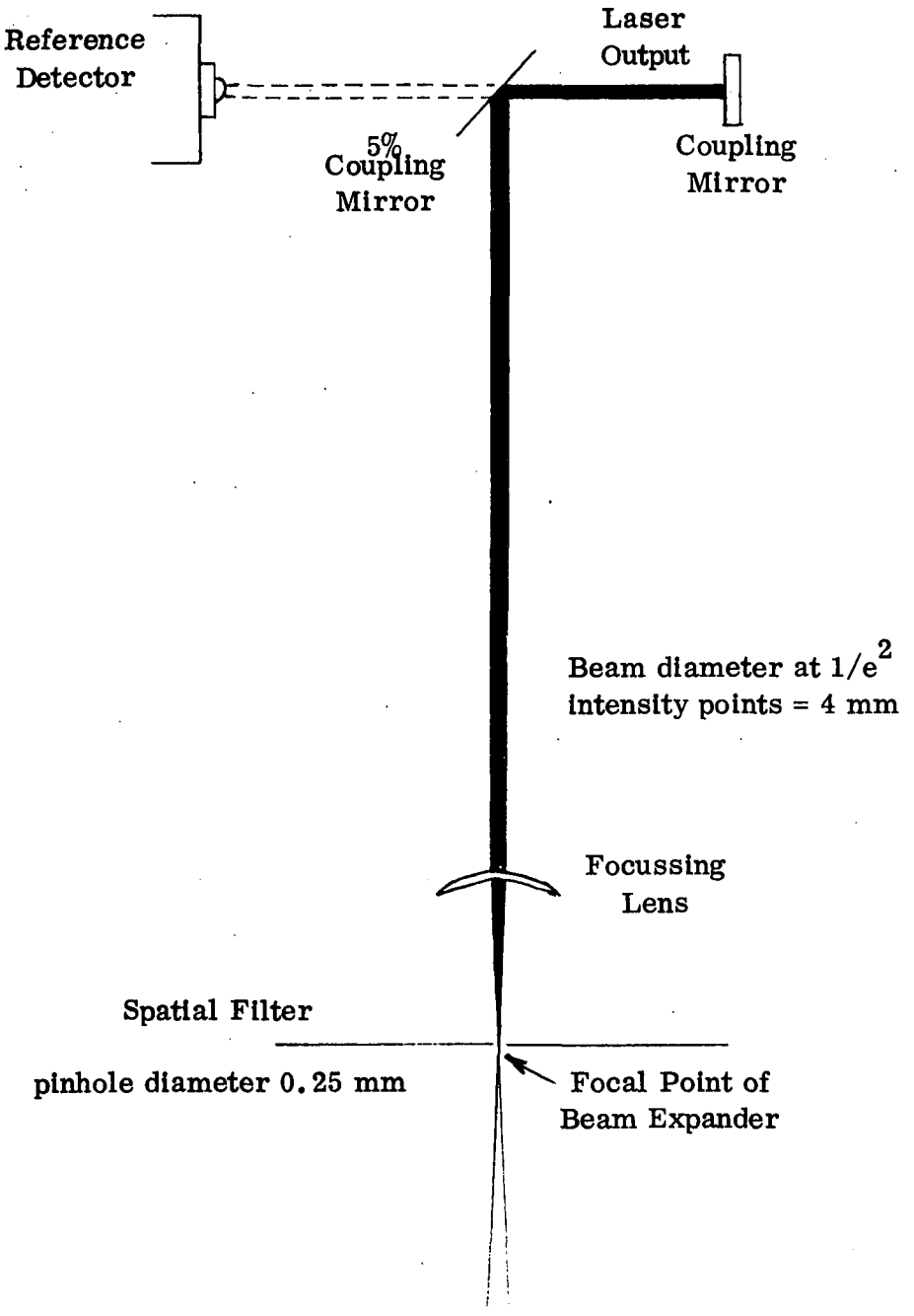

Figure 24 OPTICAL CONFIGURATION FOR SPATIAL FILTER EXPERIMENT

was a 0.25 mm aperture providing a spatial cutoff frequency of 0.4 cycles/centimeter at the beam expander output. As the figure shows, the filter provided smoothing of the higher spatial frequencies in the beam without adding appreciable beam spreading.

Figures 25 through 30 show the same one-dimensional plots using the external optics for the ILAMS system shown in Figure 33. These plots show the effects of the spatial filter (cleanup aperture), laser intracavity mode (IRIS) stop and the beamsplitter on three wavelengths, 9.305, 9.504 and 10.532 microns. Table 8 shows the conditions for each of the experiments. Comparison of the odd figures with the even figures shows the effect of the cleanup aperture. In this case the spatial frequency cutoff of the aperture is seven cycles per meter which is sufficient to produce some spreading of the beam at the beam expander output. In spite of this fact the aperture seems to have negligible effect on the high spatial frequency fluctuations of the laser power density. The conclusion therefore is that the spatial fluctuations observed are produced by the optical elements between the spatial filter and the beam expander output. Comparison of Figures 25 and 26 with Figures 27 and 28 shows that the smaller mode stop size has relatively little effect on the fluctuations in the relative power density which simply says that the 8.7 mm mode stop aperture was sufficient to maintain fundamental mode operation in the laser. Comparison of Figures 29 and 30 with the other figures shows the effect of the beamsplitter (Figure 33) in producing the laser power density fluctuations in the output. An important fact to note here is that pattern changes with wavelength. Note also that some spatial variations remain which must be attributed to the other optical elements between the cleanup aperture and the beam expander output.

In response to the results of beam mapping experiments a radical beam propagation optics configuration change was tried. The experimental

Table 8

EXPERIMENTAL CONDITIONS FOR ONE-DIMENSIONAL PLOTS

Figure #	0.9 mm Diameter Clean Up Aperture	Mode Stop Size	Beam-splitter
25	Out	8.7 mm	In
26	In	8.7 mm	In
27	Out	6.4 mm	In
28	In	6.4 mm	In
29	Out	6.4 mm	Out
30	In	6.4 mm	Out

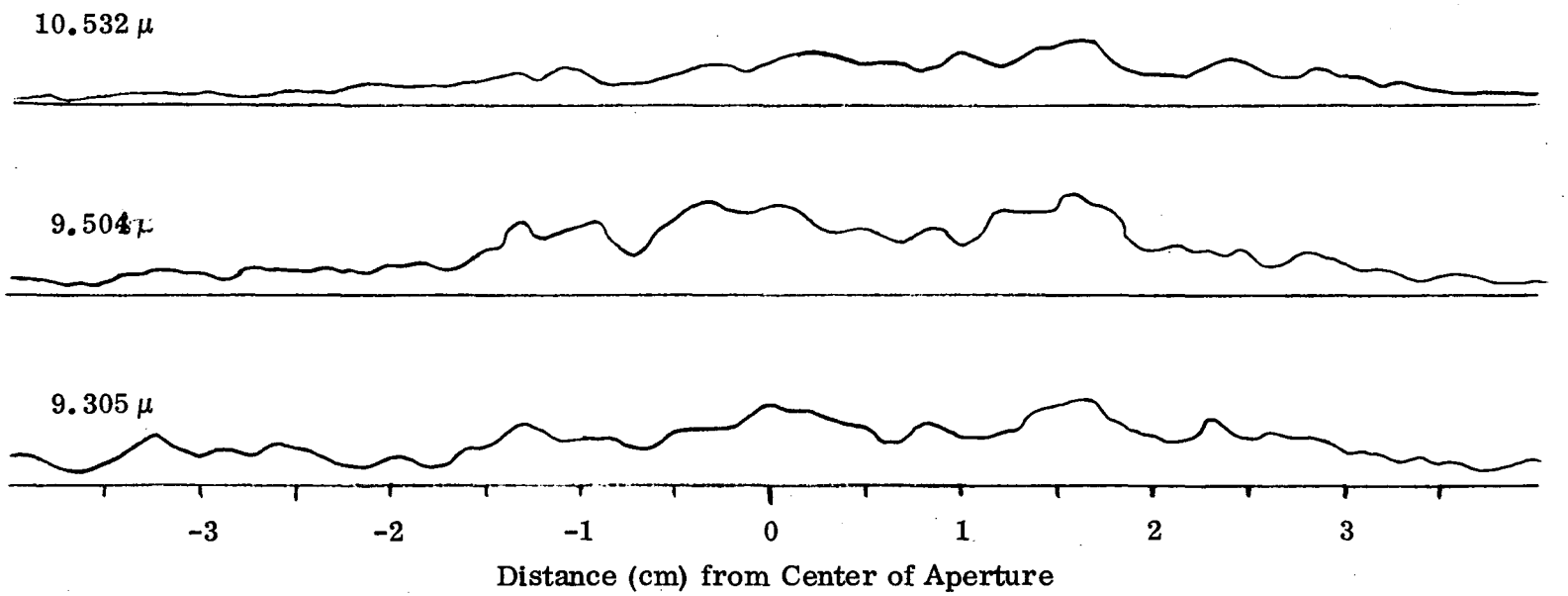

Figure 25 HORIZONTAL SCAN WITH 8.7 mm MODE STOP AND BEAMSPLITTER IN PLACE

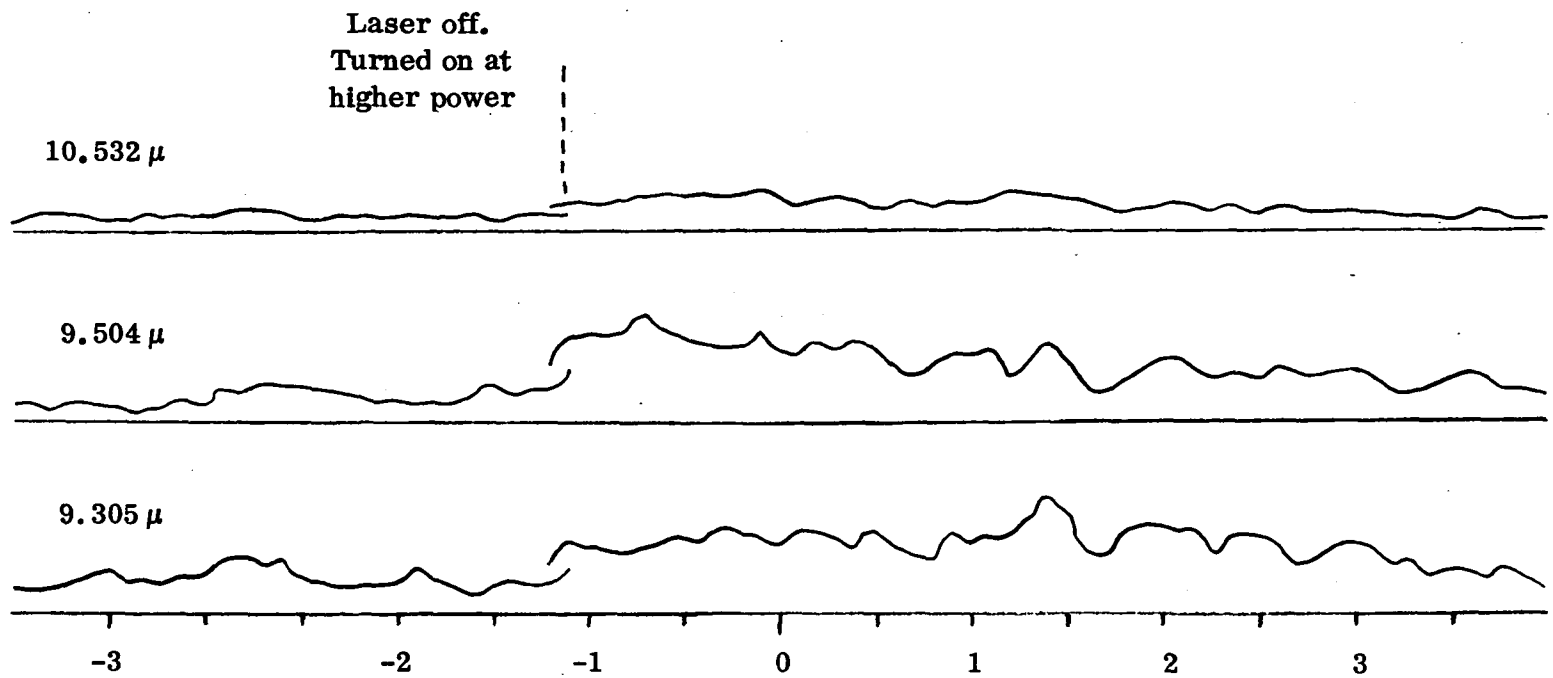

Figure 26 HORIZONTAL SCAN WITH 0.9 mm CLEANUP APERTURE, 8.7 mm MODE STOP AND BEAMSPLITTER IN PLACE

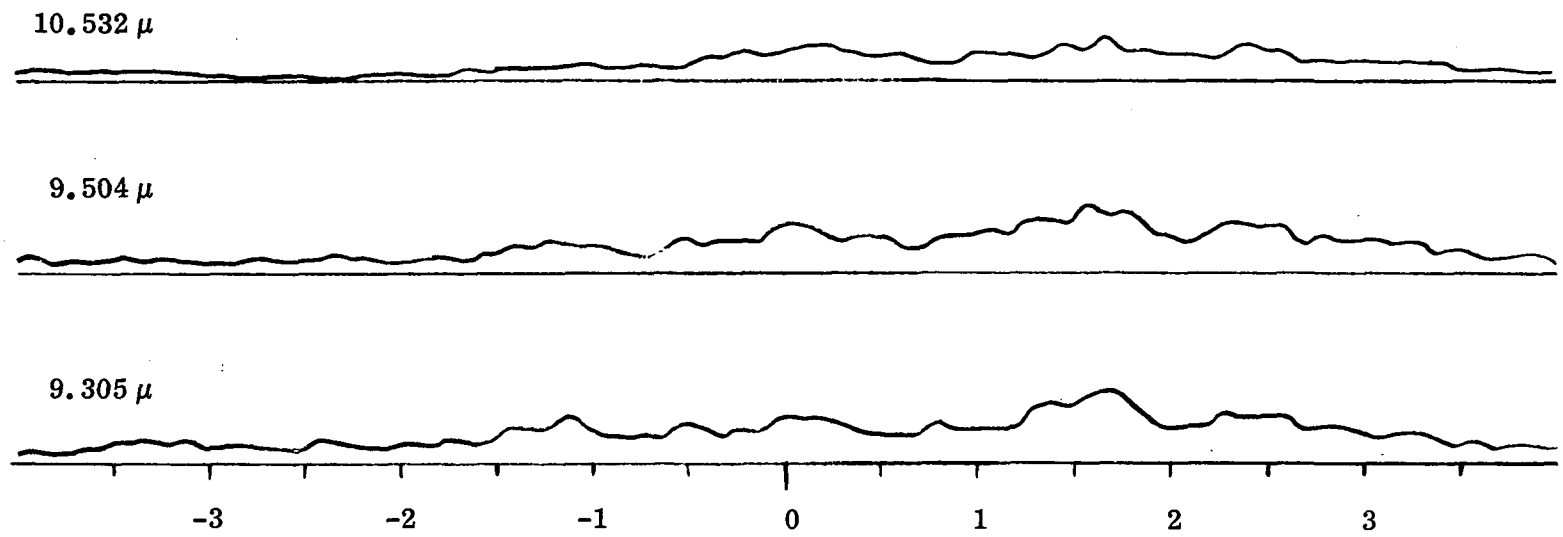

Figure 27 HORIZONTAL SCAN WITH 6.4 mm MODE STOP AND BEAMSPLITTER IN PLACE

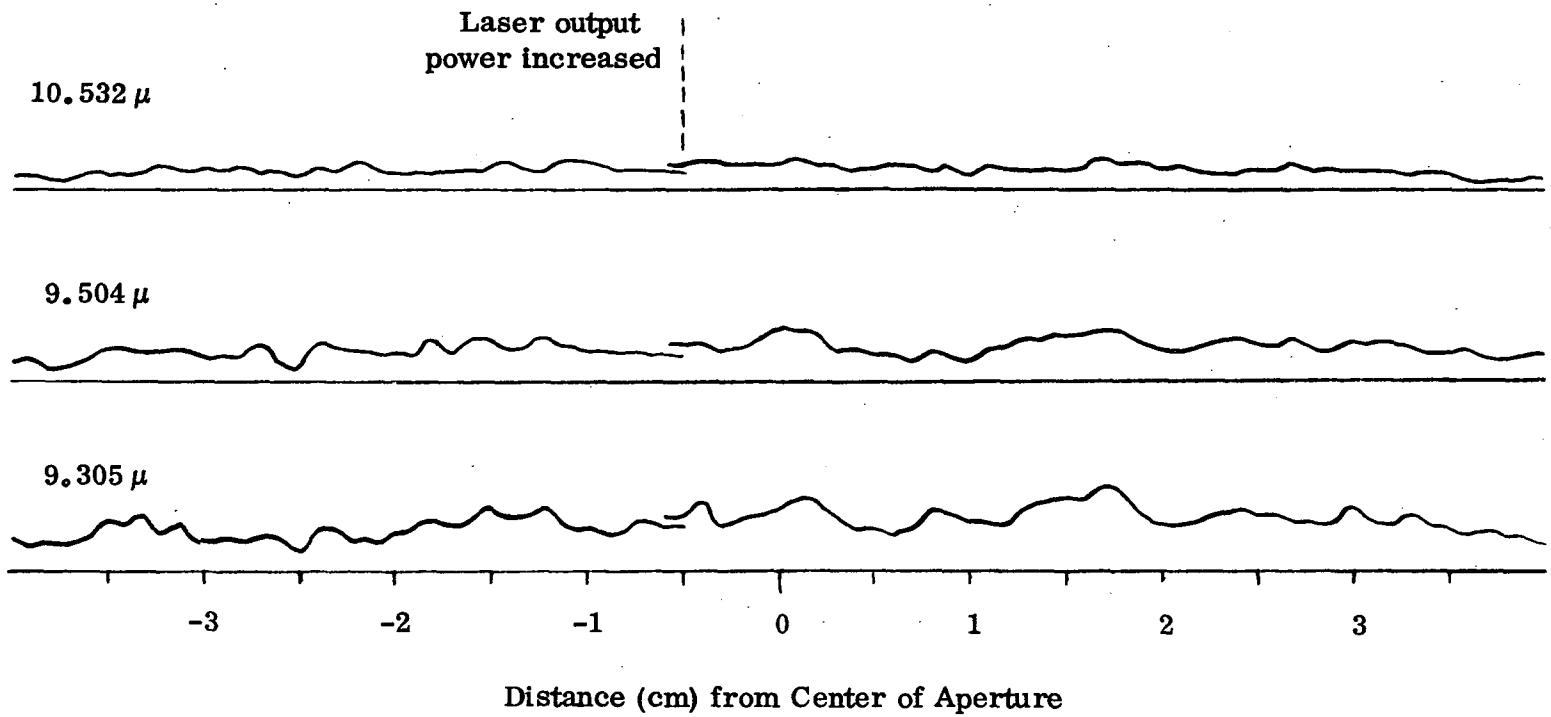

Figure 28 HORIZONTAL SCAN WITH 0.9 mm CLEANUP APERTURE, 6.4 mm MODE STOP AND BEAMSPLITTER IN PLACE

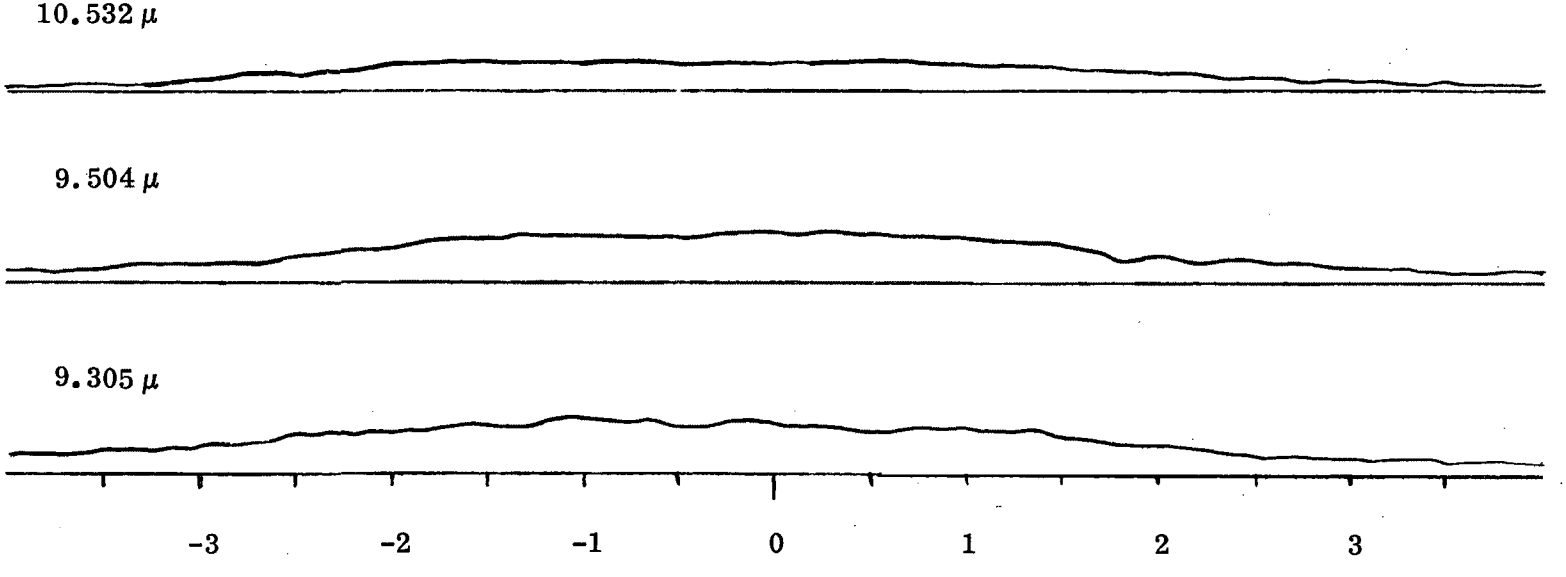

Figure 29 HORIZONTAL SCAN WITH 6.4 mm MODE STOP AND BEAMSPLITTER REMOVED

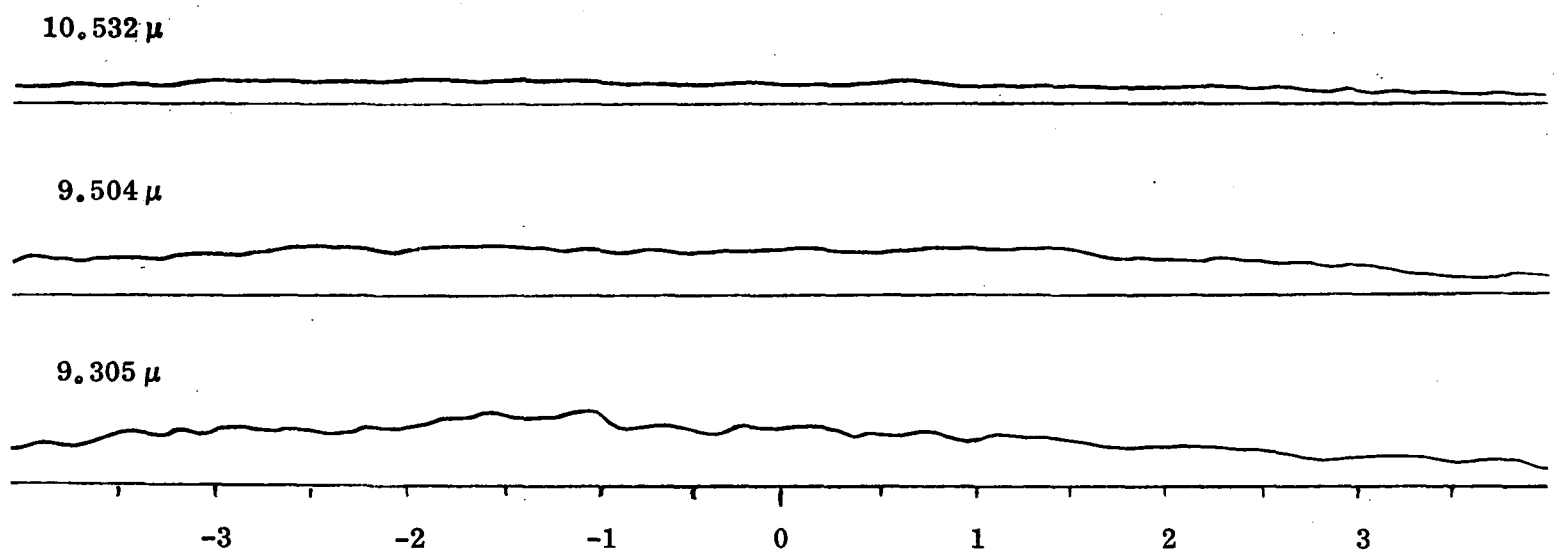

Figure 30 HORIZONTAL SCAN WITH 0.9 mm CLEANUP APERTURE, 6.4 mm MODE STOP AND BEAMSPLITTER REMOVED

configuration is shown in Figure 31. The laser beam from the coupling mirror goes to a beamsplitter. A portion of the beam passes through it to a reference detector. The balance is reflected off the beamsplitter to a spatial filter, through a hole in an angled mirror thence to the off-axis parabola (collimator) and out to the retroreflector. Returned energy comes back through the collimator and is reflected off the angled mirror with a hole in it to the signal detector. It was thought that this approach, eliminating a beam splitter after the spatial filter would improve system performance. But in the absence of clearly superior initial performance as determined by the stability of the teletype printout, further study of this configuration was halted to conserve time and funds. Beam propagation optics were returned to the original configuration.

OTHER OBSERVATIONS

An uncertainty in St. Louis measurements was the calibration of the chemiluminescent point monitor. Reference 5 reports significant concerns in this area. The portable monitors used in the reported study were made available for this program. The study concludes in part:

> "The major problem encountered in this study is the variation in the sensitivities of the monitors. The RAMS (Regional Air Monitoring System) monitors varied in total from 360 ppb to 120 ppb full scale. Of course, once the stations are fully operational this may not be the case. However, one of the mobile monitors once varied from 200 ppb at 10 AM to 133 ppb at 4 PM. As a consequence of the wide fluctuations in sensitivity, at least half of the measurement and data reduction efforts were spent calibrating and determining sensitivities."

The determination of the cause (an apparent temperature sensitivity was noted in the course of the work) of the portable (mobile) monitor fluctuations is the object of a current investigation. The report estimated that "in addition to the

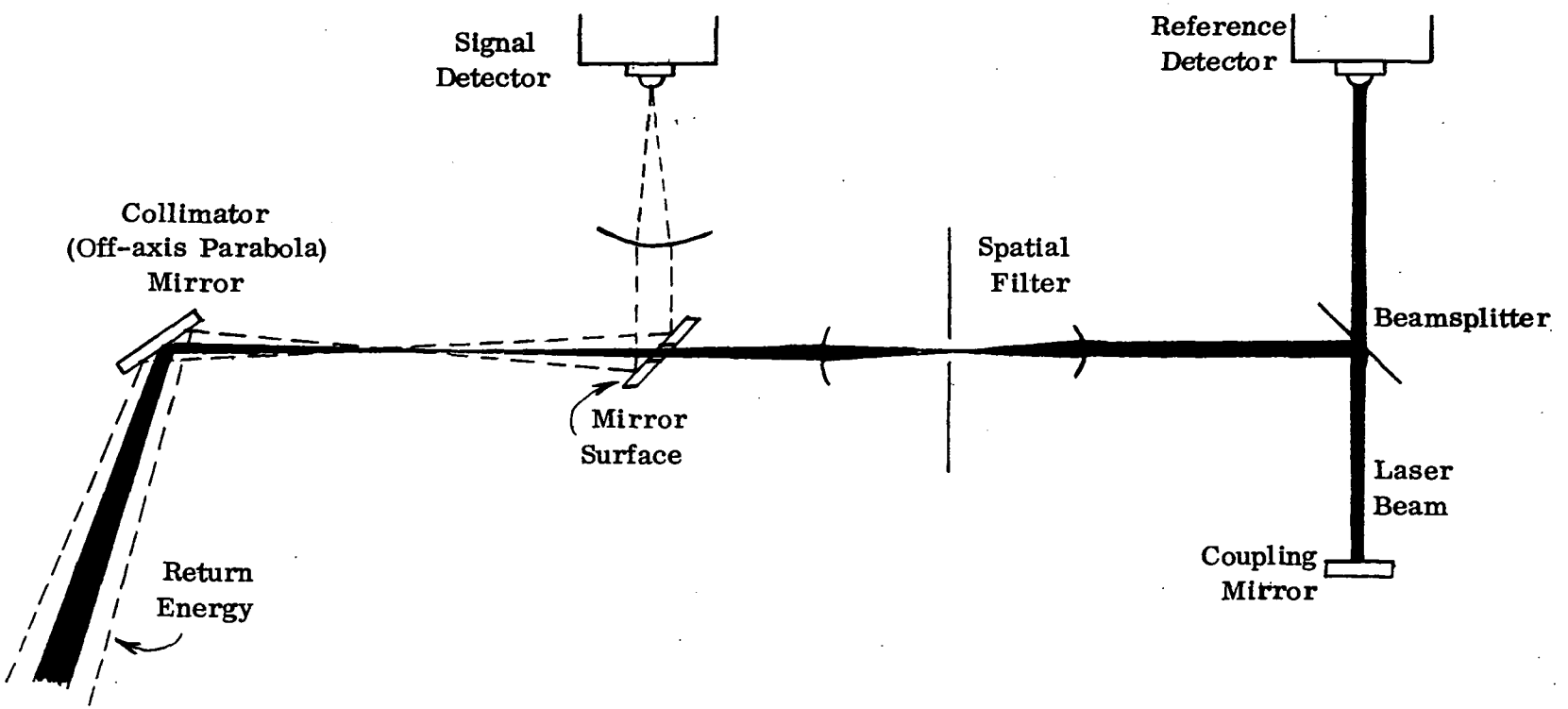

Figure 31 EXPERIMENTAL BEAM PROPAGATION OPTICS CONFIGURATION

uncertainties arising due to the fluctuation in the ozone concentration, there is an additional error of at least ±5% due to uncertainties in calibration."

REFERENCES

1. Snowman, L. R., et al. "Development of a Gas Laser System to Measure Trace Gases by Long Path Absorption Techniques" Final Report, EPA Contract 68-02-0757, June 1974.

2. Morgan, D. R. and Roberts, D. A., "Computer Signal Processing Study", Dept. of the Army DDEL, Final Report, Vol 1: Analytical Results Contract DAAA15-71-C-0186, September 1972.

3. Kreuzer, L. B., Kenyon, N. D., Patel, C. K. N., "Air Pollution: Sensitive Detection of Ten Pollutant Gases by Carbon Monoxide and Carbon Dioxide Lasers" SCIENCE VOL 177, pp 347-349, 28 July 1972.

4. Snowman, L. R., "Field Study on Application of Laser Coincidence Absorption Measurement Techniques" Final Report of EPA Contract EHSD 71-8.

5. Chaney, L. W. and McClenny, W. A., "St. Louis Regional Air Pollution Study Sub-Grid Scale Characterization Pollutant Distribution Study" Preliminary Draft.

Appendix A
ILAMS SYSTEM DESCRIPTION

The Infrared Laser Atmospheric Monitoring System (ILAMS) operates in the middle region of the infrared spectrum and identifies atmospheric constitutents by absorption spectroscopy. It measures average pollutant concentrations (total burden) over its optical path. Laser operation is at relatively low, safe power densities of .001 to .01 watts/cm^2 in the spectral region where the eye does not transmit.

Figure 32 shows a block diagram of ILAMS. The output power from the laser is directed to a 50% beamsplitter via a 1 mm spatial filter (cleanup aperture). The energy reflected from the beamsplitter is focused down to a 0.1 mm aperture which serves as an attenuator. Behind this aperture is the reference energy detector. The transmitted power through the beamsplitter goes to a germanium lens which focuses the energy near the focal point of an off-axis parabolic mirror, and the expanded, nearly collimated beam is transmitted to the retroreflector. The return energy from the retroreflector retraces the path through the beam-expanding parabolic mirror and the germanium lens to the beamsplitter. The return energy reflected from the beamsplitter is collected by a germanium lens doublet and focused on the signal detector. Preamplifiers are mounted directly behind the signal and reference detectors and their outputs go to the signal processor. The detectors used in the system are thermistor bolometers, operating at ambient temperature (uncooled), having a characteristic flat response across the middle IR spectral region.

In the signal processor, the natural logarithm of the return to reference signal ratio is taken for each wavelength. These logs are weighted and summed to produce an output proportional to pollutant concentration in accordance with Beer's Law principles. Transmitted wavelengths are selected with the aid of computer programs using system parameters and absorption coefficient data for target gases and expected interferences, to maximize return signal to noise ratios. Linear weights are computer-calculated to discriminate pollutant effects from interferences.

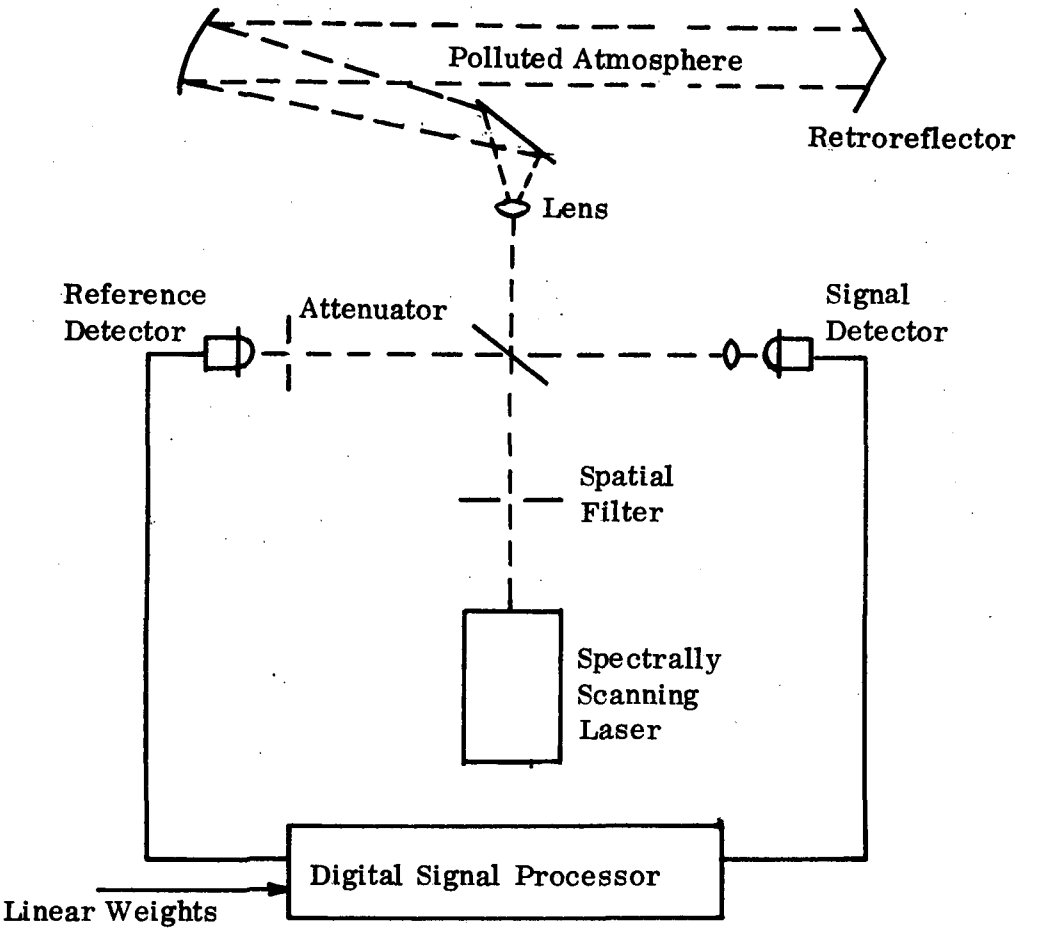

Figure 32. ILAMS BLOCK DIAGRAM

The CO_2 laser in the system is alignable to six wavelengths. These wavelengths may be selected from the more than 70 available with $C^{12}O_2^{16}$. The laser is presently designed to detect ozone, ethylene and ammonia in an environment that is expected to contain neutral attenuation, carbon dioxide and water vapor as spectral interferences. With other isotopes of CO_2 or other gas lasers the system has the potential for detecting practically all important pollutants. The spectrally scanning laser itself includes a high-gain flowing gas CO_2 laser as the radiation source and a wavelength selection mechanism, which periodically (40 Hz) scans through a series of six laser wavelengths. The laser optical configuration is shown in Figure 33. The laser cavity consists of a "V" shaped plasma tube and an external spectral tuner. A relatively long laser cavity is used for sufficient gain to overcome the losses inherent in the spectral tuner and to obtain lasing action on a large number of spectral lines. A beam travels through the plasma tube with aid of a mirror at the point of the "V". Leaving the tube through a germanium Brewster window, the beam is directed by mirrors through an iris (for mode control) and onto a 105 lines/mm diffraction grating, which disperses the beam spectrally and spatially. The six wavelengths of interest are then relayed through holes in the chopper wheel to the four end mirrors of the laser cavity. These holes in the chopper are so located that, as the wheel turns, only one wavelength at a time is permitted to pass through to the end mirrors. The six end or wavelength selection mirrors are adjusted so that the beams are directed back on themselves through the laser cavity. In this way, selected laser wavelengths are transmitted sequentially.

The mini-computer signal processor includes a general purpose (stored program) mini-computer and appropriate interface electronics. The collection and reduction of data is entirely under computer, i.e., program control; results are displayed on simple displays incorporated in the equipment, and on an optional teletype, which need not be used (or even be connected) during field or test range exercise of the system.

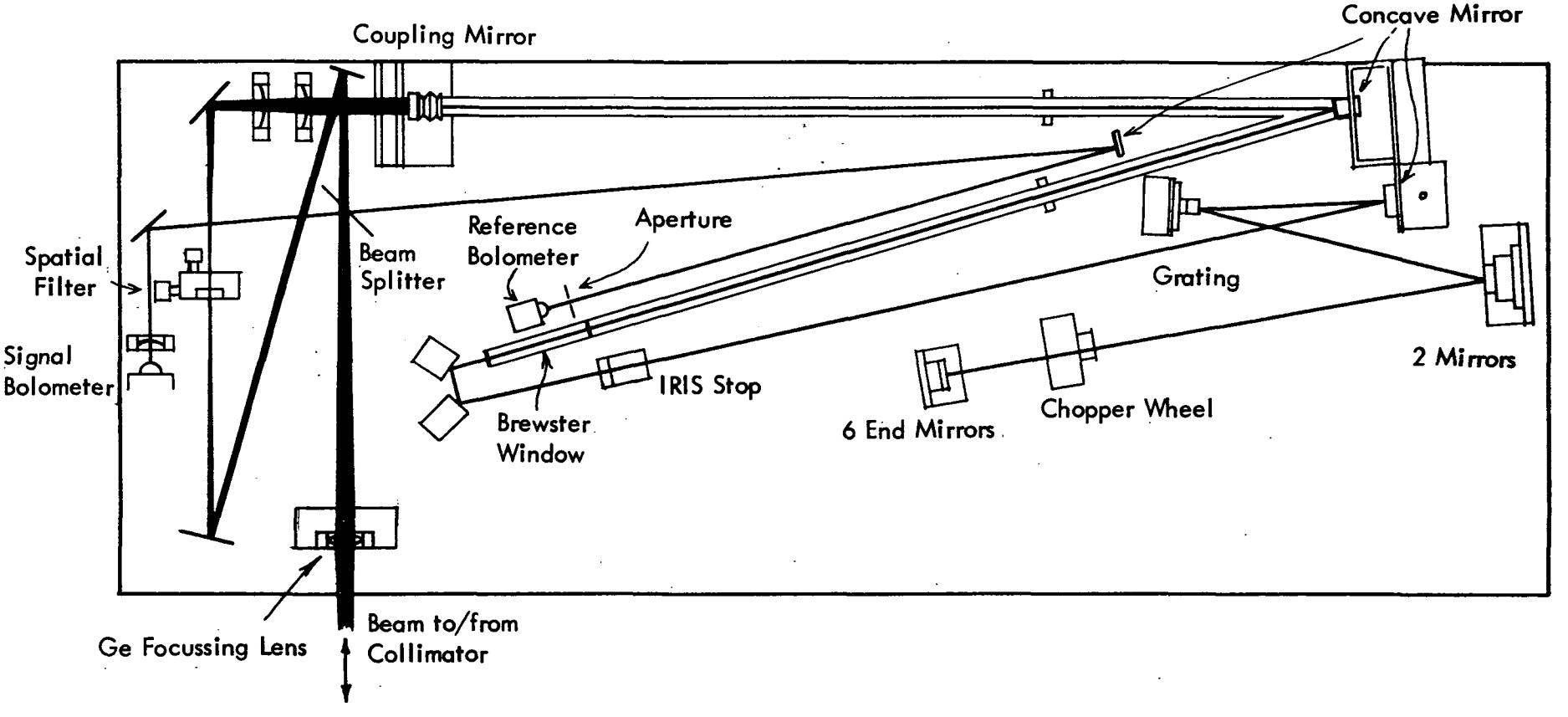

Figure 33. "V" LASER OPTICAL LAYOUT

The use of the stored program control and data reduction means:

- changes in system design, or variations in data reduction algorithms, may be accommodated without alteration of the data collection or reduction hardware; only changes in the control program will be required.

- modification of signal processor parameters such as number of wavelengths (up to 8), gate locations, system response time, weighting factors, etc., do not even require software changes, these parameters are expediently entered by the teletype input.

- the precision of data processing may be made as accurate as desired; similarly the impact of imprecise calculations may be assessed by direct simulation for purposes of evaluating future low cost special purpose instruments.

- additional data, e.g., environmental conditions, time, date, signal variability, laser parameters, etc., may be measured and recorded without modification of or addition to the existing system hardware.

- the performance of one or more data processing and display systems can be directly analyzed, e.g., data from several ozone monitors could be crosscorrelated and recorded.

The data collection and reduction system is sketched in Figure 34. A Digital Equipment Corporation PDP 11/05 is used for the central processor. The data collection and reduction equipment in Figure 34 consists of three major subsystems:

Interface Subsystem

This subsystem includes an 8 input analog signal multiplexer, which is followed by a sample-and-hold amplifier and an analog-to-digital converter at 10-bit precision. (The analysis path detector preamplifier output is connected to one multiplexer input, the reference path to a second multiplexer input, the remaining 6 are available for sensing other voltage levels of interest). Additional subsystem elements include an AGC attenuator, a wheel position counter and demultiplexer/storage capability for analog data displays like the meters shown in Figure 34.

Central Processor Subsystem

The central processor and its own control panel form this subsystem. Power supplies for this equipment are contained within the CPU cabinet proper. The central processor control panel ordinarily is disabled during operation.

Program Input and Data Logging Subsystem

A Teletype Corporation ASR-33 teletype with appropriate interface circuits constitutes this subsystem. As indicated, it plays two roles. First, it permits entry (ordinarily via paper tape) of the control program. Second, it permits detailed reporting of directly measured quantities, or derived (computed) quantities.

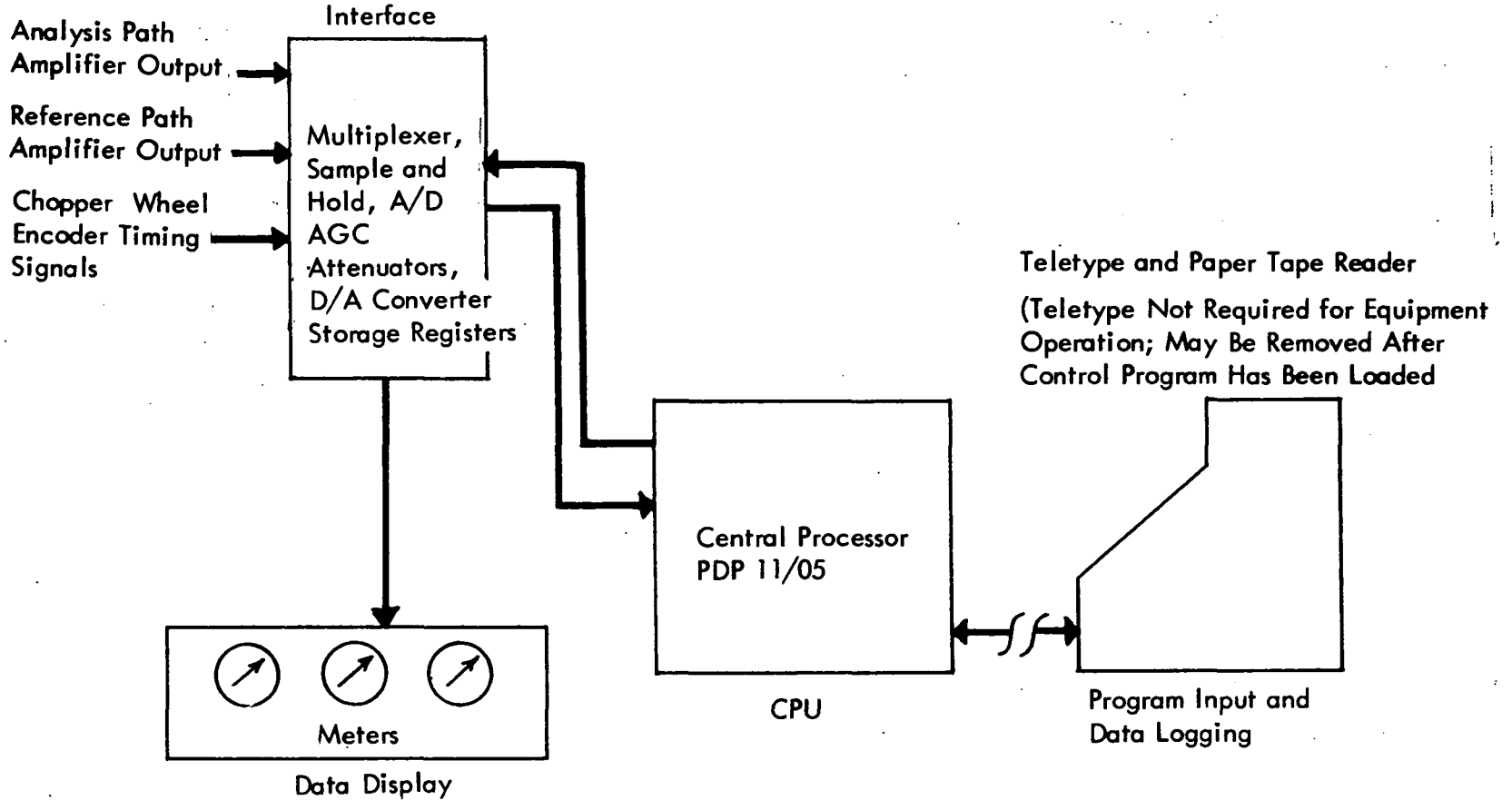

Figure 34. DATA COLLECTION AND REDUCTION SYSTEM

The central processor is designed so that programs stored in its core memory may be caused to remain intact during periods of no primary power. This option is exercised, so that once a control program has been entered in the CPU, it need not be reentered until there is a need to change it, regardless of whether the CPU remains energized or not. The control program is designed so that it will run properly regardless of whether the teletype is connected or not. Thus the teletype unit is an optional data display device, not an essential component of the system once the control program has been entered.

The present system is in a breadboard configuration and is housed in a 2.4 by 4.8 meter (8 x 16 ft.) mobile office-type trailer. Beam steering capability allows the laser beam to be positioned 360° in azimuth and ±10° in elevation. The system is shown in Figure 35. The laser is in the background and before the seated operator is the PDP 11/05 Computer (central processor) and output meters. The interface unit is out of sight behind the computer and output meters. The ASR 33 teletype is in the foreground.

Figure 36 shows the beam steering optics, the present location of the laser in the trailer, and the structure over the laser extending through the trailer roof to support the upper beam steering mirror. The long gray cylinder whose base is prominent near the center of the figure houses the off-axis parabolic mirror used as the transmit-receive optics. Behind the gray cylinder can be seen the lower beam steering mirror and in it, the reflection from the upper mirror and a portion of the fixture (black ring) supporting it.

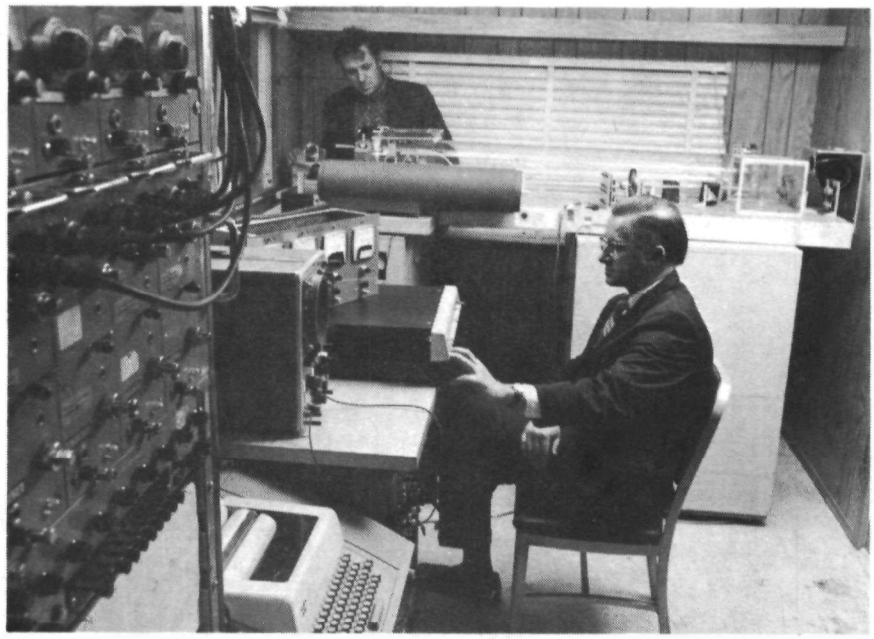

Figure 35. BREADBOARD SYSTEM

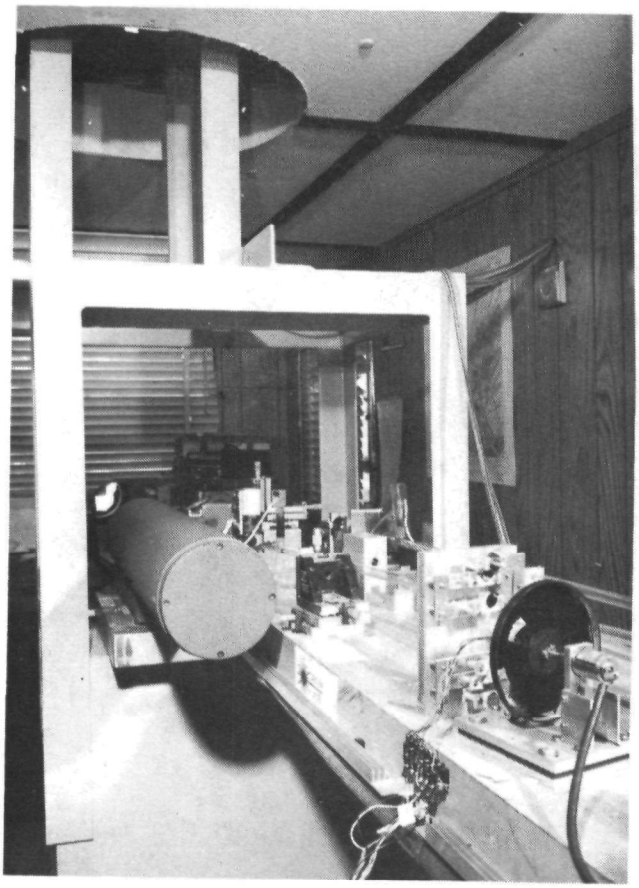

Figure 36. BEAM STEERING OPTICS

Appendix B

POLLUTANT CONCENTRATIONS DETECTABLE WITH GAS LASER LONG PATH SENSORS

An indication of pollutant concentrations detectable at present and projected ILAMS sensitivities can be obtained from calculations. The results of this work have been summarized in Table 9. System sensitivity to 1% absorptions means that all important pollutants are detectable in average (integrated) concentrations of 1 to 15 ppb over a 1 kilometer range. If another order of magnitude (0.1% level) improvement in sensitivity can be attained, average concentrations varying from 0.1 to 1.5 ppb of such pollutants as CO, NO, NO_2, SO_2 and O_3 are detectable over a 1 kilometer range. This distance (2 kilometers out and back) represents the minimum "optical thickness" required for the indicated concentration levels. A longer monitoring range will also enhance sensitivity in direct relation to the increased path length. (There is, however, a limit to this means of sensitivity improvement as will be seen later.)

The information in Table 9 is calculated with pollutant spectral data using Beer's Law relationships. Assuming that the line width of the resonance absorption is broad compared to the transmitted laser line width, and assuming also that there is no saturation in the absorbing media, then, for a uniform concentration of the absorber over the path, the transmission at each discrete wavelength is of the form:

$$T_m = \exp(-A_m C_A L) \qquad (1)$$

where A_m is the absorption coefficient of absorber A at transmitted wavelength m, C_A is the concentration of absorber, A, over the total optical path, and L is the total optical path through the sample region. If the concentration is non-uniform over the path, as is usually the case, then $C_A L$ can be

Table 9

Indicated ILAMS Pollutant Detectability for a

Laser to Retroreflector Range of One Kilometer

(Two kilometers total path)

Pollutant	Minimum Detectable Concentration in Parts per Billion	
	1.0% (1)	0.1% (1)
SO_2	4	0.4 -HeNe
	94	9.4 -$C^{12}O_2{}^{18}$
CO	15	1.5
O_3	4	0.4
NO_2	13	1.3
NO	10	1.0
NH_3	2	0.2
C_2H_4	2	0.2
H_2S	1345	134.5
HCl	1515	152
HNO_3	4	0.4
HCHO	27	2.7
PAN	11	1.1
PBzN	1	0.1

(1) Projected system sensitivity in terms of percent absorption

replaced by the integrated concentration over the total path. Typically, C has units of grams/liter or atmospheres of partial pressure, and L is in centimeters. A_m is in units to make $A_m C_A L$ dimensionless.

A little manipulation simplifies calculations and converts equation (1) to a form consistent with sensitivity terms:

$$\ln\left(\frac{1}{T_m}\right) = A_m C_A L \qquad (2)$$

In this expression, the righthand side is equivalent to another frequently used sensitivity term, αCL, which is usually displayed directly on the system's teletype printout for each target gas. In this expression α is the absorption coefficient, C the average concentration and L path length. Also, since transmission = 1 - absorption, small absorption values are approximately equal to $\ln(\frac{1}{T})$, and translate almost directly into αCL or $A_m C_A L$. Thus, αCL's of 0.1, 0.01, and 0.001 are treated as equivalent respectively to absorptions of 10%, 1%, and 0.1%.

It can be seen from equation (2) how the Table 9 concentration levels (C_A) for a 1 km system range (2 km total path) are calculated for 1% and 0.1% absorptions once A_m is determined. The absorption coefficient values used in Table 9 calculations appear in Table 10 . Because laser line widths are orders of magnitude narrower than the resolution of spectra generated by conventional spectrophotometers, it is desirable to obtain absorption coefficients from actual laser measurements with the gas of interest at the selected line (laser wavelength). Wherever known, such data was used. For some pollutants, however, it was necessary to calculate A_m using equation (2) and scaling an approximate value of T_m at the selected laser wavelength from a conventional absorption spectrum. Data sources for each gas are noted in the Remarks column of Table 10 and referenced at the end of this Appendix.

Table 10

Absorption Coefficient Data for Indicated ILAMS

Pollutant Detectability

Pollutant	A_m Absorption Coefficient (atm^{-1})	Wavelength (Microns)	Laser	Remarks
SO_2	13.23	7.427	HeNe	Laser measurement
	.53	9.024	$C^{12}O_2^{18}$	Laser measurement (1)
CO	3.329	4.6110	HeXe	Laser line from Table 5-15 (2) Spectrum from Beckman IR-9
O_3	12.7	9.501	CO_2	Laser measurement (3)
NO_2	3.965	3.448	HeNe	Laser measurement
NO	5.123	5.4048	HeNe	Laser measurement
NH_3	21.9	10.331	CO_2	Laser measurement (3)
C_2H_4	29.10	10.529	CO_2	Laser measurement (3)
H_2S	.0372	7.6510	HeNe	Laser line from Table 5-11 (2) Spectrum #37 p. 1231 (4)
HCl	.033	3.3344	HeNe	Laser measurement
HNO_3	14.25	11.1732	$C^{13}O_2^{16}$	Laser line Table A-2 p. 48 (5) Spectrum #36 p. 1231 (4)
HCHO	1.842	3.5080	HeXe	Laser from Table 5-15 (2) Spectrum Fig. 12 p. 115 (6)
PAN	4.750	10.7250	$C^{13}O_2^{16}$	Laser line Table A-2 p. 48 (5) Spectrum Fig. 29 p. 134 (6)
PBzN	40.99	10.120	$C^{13}O_2^{16}$	Laser line Table A-2 p. 48 (5) Base 10 absorption coefficient(7)

The effect of an increase in monitoring range can also be seen from equation (2). For given values of T_m and A_m, a larger L means a lower detectable concentration. A one-way optical path of a kilometer, produced by 1 kilometer separation of laser and retroreflector or by path folding over shorter distances, represents the minimum optical thickness (concentration-path length product) required to produce sufficient signal for detection of the indicated concentration levels. Monitoring range can thus be increased to the limit of atmospheric attenuation and, ultimately, detector noise, for further sensitivity improvement (reduction in threshold concentration levels). The reduction factor equals the ratio of monitoring range to the 1 kilometer range used in calculations. For example, the 3 mile range over which we operated in Syracuse would reduce system threshold (minimum detectable) concentration levels by a factor of about five.

REFERENCES

1. Menzies, Robert T., "Remote Detection of SO_2 and CO_2 with a Heterodyne Radiometer", Appl. Phys. Lett. Vol 22, No. 11, 1 June 1973, p 592.

2. Smith, W. V., and Sorokin, P. P., "The Laser", McGraw-Hill Book Co., 1966.

3. Patty, R. R. et al., "CO_2 Laser Absorption Coefficients for Determining Ambient Levels of O_3, NH_3 and C_2H_4", Applied Optics Vol 13 No. 12 December 1974, p 2850.

4. Pierson, R. H., Fletcher, A. N., and Gantz, E. St. C., "Catalog of Infrared Spectra for Qualitative Analysis of Gases", Analytical Chemistry, Vol. 28, August 1956, p. 1218.

5. Jacobs, G. B., Morgan, D. R., Snowman, L. R., and Ware, D. A., "Spectrally Scanning CO_2 Laser Design Considerations", G. E. Technical Information Series Report R67ELS-94, December 1967.

6. Hanst, P. L., "Spectroscopic Methods for Air Pollution Measurement", in Advances in Environmental Science and Technology, Vol. Two, John Wiley & Sons, Inc. 1971.

7. Heuss, J. M., and Glasson, W. A., "Hydrocarbon Reactivity and Eye Irritation", Environ. Sci. & Tech., Vol. 2, No. 12, p 1109, Dec. 1968.

Appendix C

LASER LONG PATH MONITORING APPLICATIONS

The results obtained to date suggest ILAMS has utility for both atmospheric monitoring and research. A block diagram of the general system concept for multi-pollutant monitoring of a large urban area is shown in Figure 37. It adds beam rotation or steering and multiple retroreflectors to the concept previously described. A spectrally scanning laser, or lasers, capable of emitting multiple wavelengths would be employed in the system. They would provide IR energy over the spectral range defined by the detection problem (3-12 microns for the pollutants listed below). While spectrally scanning lasers with CO_2, isotopic CO_2, and noble gas fill mixtures have been used in laboratory and field experiments, the system is adaptable to tunable lasers employing other media. Rapid developments in laser technology indicate that three or perhaps only two lasers would offer sufficient lasing lines to identify important urban atmospheric pollutants as discussed in Appendix B.

A basic monitoring configuration is shown in Figure 38. An urban area, with retroreflectors located about its periphery, is swept by the optically rotated laser beam of a centrally located transceiver. With such an arrangement, the system would provide a warning when pollutant concentrations exceeded standards. At the same time, it would be gathering data useful for establishing ambient or baseline pollutant levels for the monitored area. Similarly, finer data granularity in certain portions of a monitored area can be obtained with intermediate retroreflectors. With pollutant concentration data from the long and short paths, the pollutant contribution of the area in between can be determined.

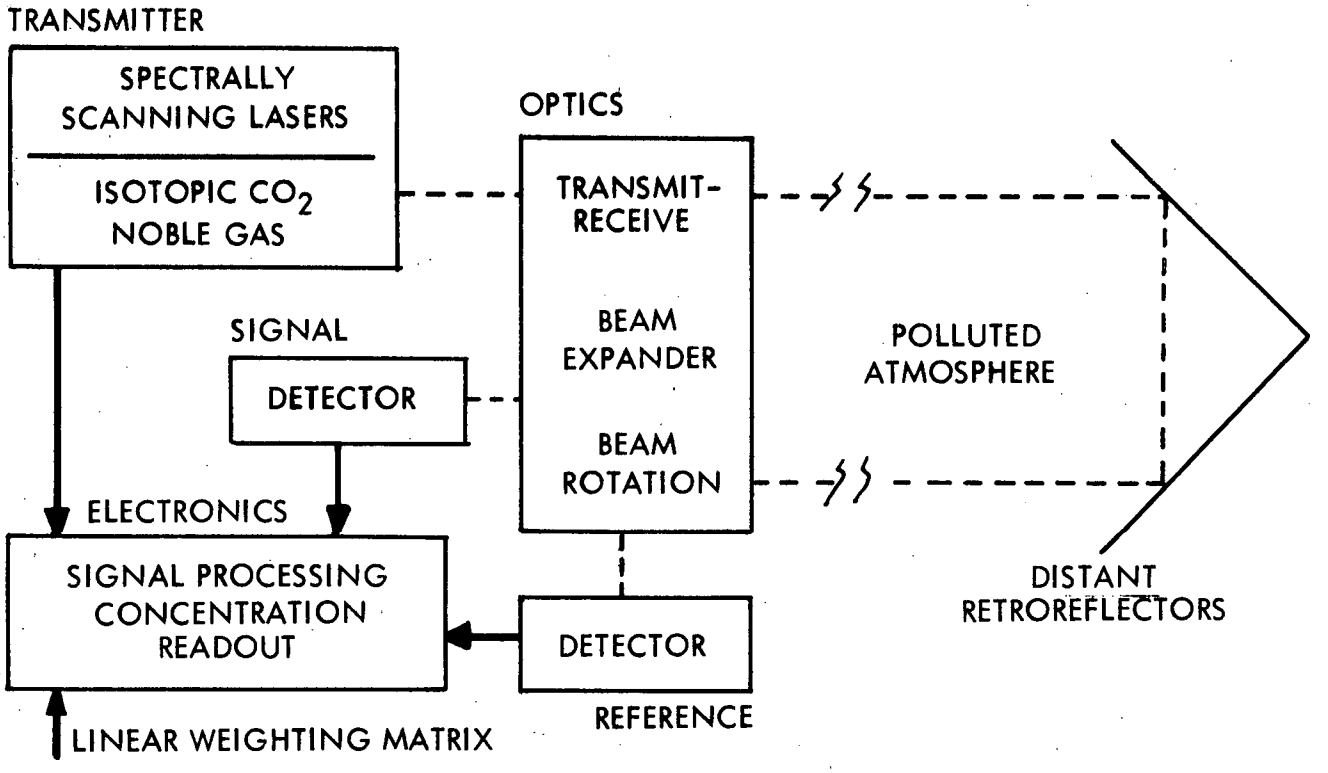

Figure 37. SYSTEM CONCEPT FOR MULTIPOLLUTANT URBAN AREA MONITORING

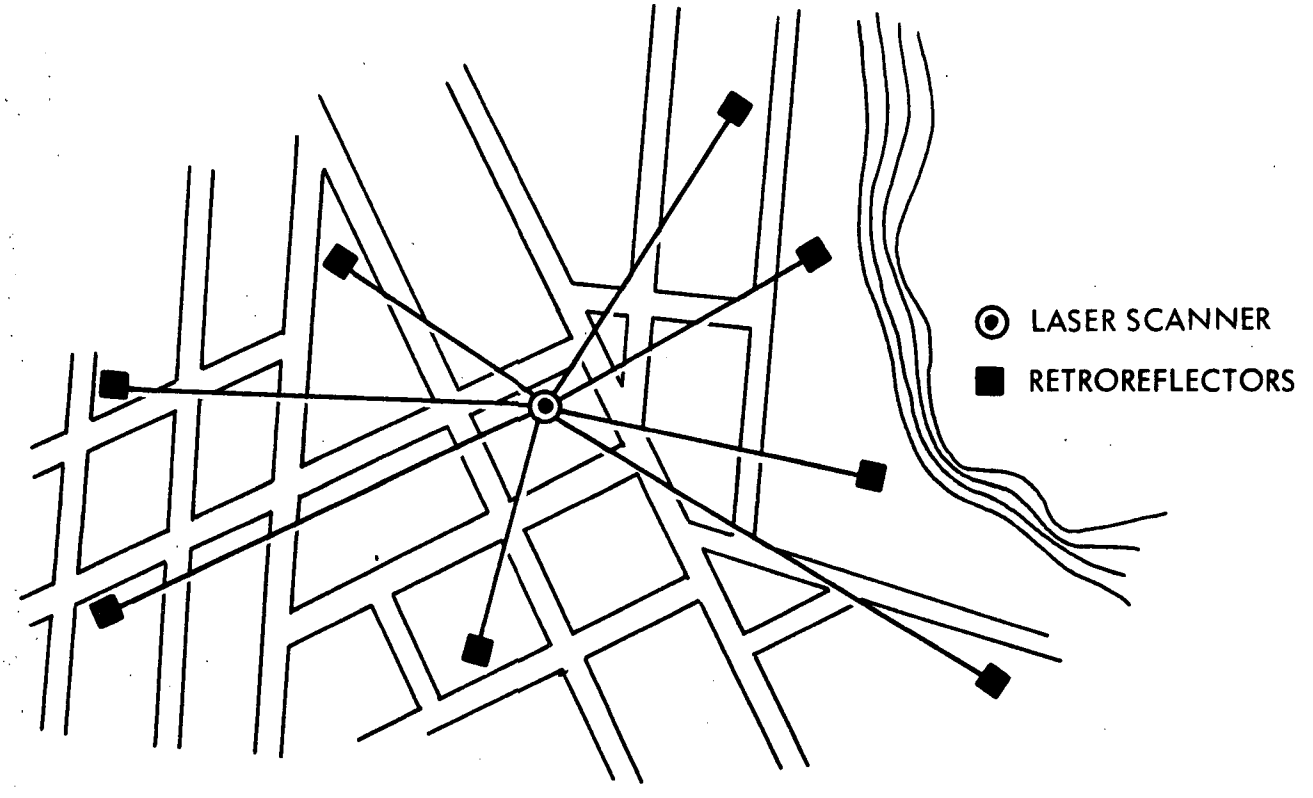

Figure 38. AREA MONITOR CONFIGURATION

It is of interest to note how the detectable pollutant concentrations of Appendix B relate to the monitoring requirements. Table 11 compares Appendix B Table 9 values with some pollution monitoring criteria. Detectable concentrations even at the 1% sensitivity level are comfortably below federal standards. The Request for Proposal leading to our field evaluation contract with EPA included suggested pollutants and concentration ranges for long path monitoring as noted in the table. It can be seen here, too, that 1% sensitivity levels are adequate. In all but one case, 1% levels are at, or below, the low end of these ranges. And even in this instance, NO_2, the discrepancy is minor, 10 ppb versus 13 ppb.

Such results can have substantial impact on monitoring philosophies. It has been suggested that long path data, average concentration over an optical path, may be more representative of pollution, especially ambient air levels. Being able to operate at the indicated low concentration levels may serve to prove this point. When applied to validation of meteorological models, long path monitor data is particularly attractive, just because it is "average." One kilometer is about the resolution limit of current models. "Resolution" in this context is the distance over which pollutant concentrations are assumed to be constant.

The comparative strengths and weaknesses of point and long path sensors for urban area monitoring have been discussed.[1, 2] Both of the referenced works cite the need for the orders of magnitude sensitivity improvement in long path monitors which the work proposed here expects to achieve. Achieving this improved performance, along with weighing the two sensor types in terms of not initial, but total cost, can resolve current cost effectiveness questions. If total costs are considered when point and long path monitoring networks are compared, then operating expenses become an important factor and the unattended operation feature of optical sensors is significant. It may well tip the balance of cost effectiveness in favor of long path sensors.

Table 11

Comparison of Indicated ILAMS Pollutant Detectability

with Pollution Monitoring Criteria

(All data in parts per billion)

Pollutant	Minimum Detectable Concentration		Suggested Monitoring Range[2]	Federal Standard
	1.0%[1]	0.1%[1]		
SO_2	4	0.4	10 - 1,000	140[3] (max. 24 hr. conc.)
CO	15	1.5	500 - 50,000	9000[3] (max. 8 hr. conc.)
O_3	4	0.4	10 - 1,000	80[3][4] (max. 1 hr. conc.)
NO_2	13	1.3	10 - 1,000	50 (annual arith. mean)
NO	10	1.0	10 - 1,000	
NH_3	2	0.2	50 - 500	
C_2H_4	2	0.2	10 - 500	

(1) Projected ILAMS sensitivity in terms of percent absorption

(2) From RFP No. CPA - Neg. 221, "Field Study on Application of Laser Coincidence Absorption Measurement Techniques."

(3) Not to be exceeded more than once per year

(4) Photochemical oxidants

To meet particular monitoring and research requirements, a number of configurations are possible. Figure 39 illustrates a configuration to obtain finer data granularity with retroreflectors positioned to obtain long and short path data. For survey work, a trailer configuration such as that shown in Figure 40 is convenient. For the urban portion of the EPA evaluation program and subsequent programs, the system was employed in this way. Emplaced or portable retroreflectors could be used, depending upon the nature of the survey. Perimeter monitoring of a high-emission multiple source area is envisioned with the component arrangement of Figure 41. The concept shown in Figure 42 proposes vertical monitoring with an airborne retroreflector and the laser transceiver on the ground. Other arrangements for vertical monitoring are also possible.

A folded path configuration, Figure 43, is useful for plume studies or to detect pollutants whose absorption strengths are not compatible with available monitoring range (line of sight) for a particular installation. Folded path configurations provide ILAMS with quasi-point monitoring capability to localize pollution sources either as a separate unit or as part of a larger network similar to the intermediate retroreflectors of Figure 39.

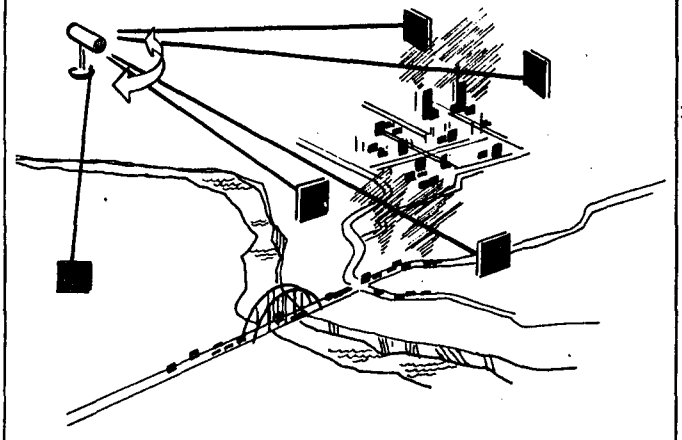

Figure 39. SENSITIVE SECTOR MONITOR

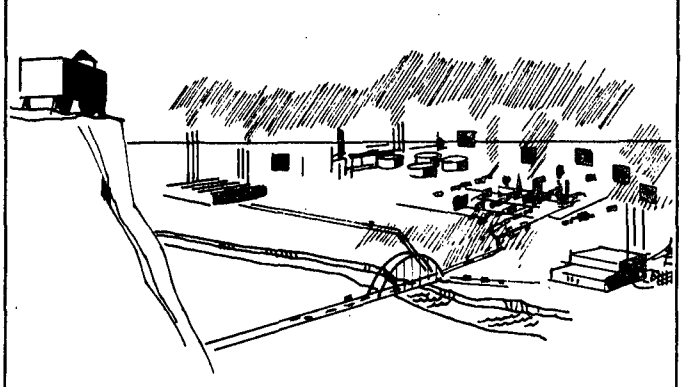

Figure 40. MOBILE MONITOR

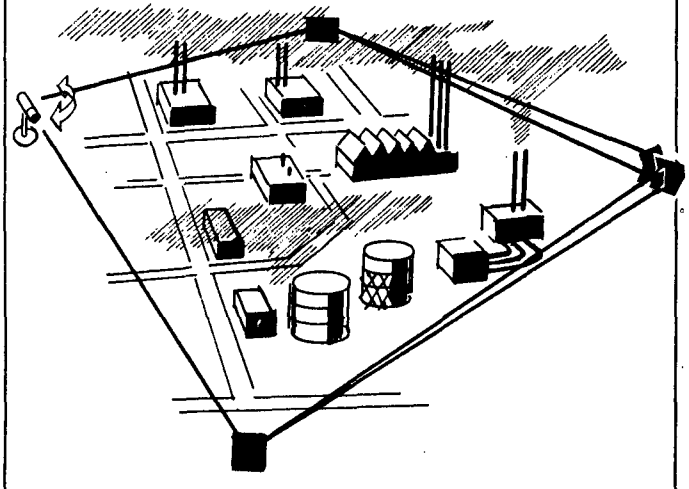

Figure 41. PERIMETER MONITOR

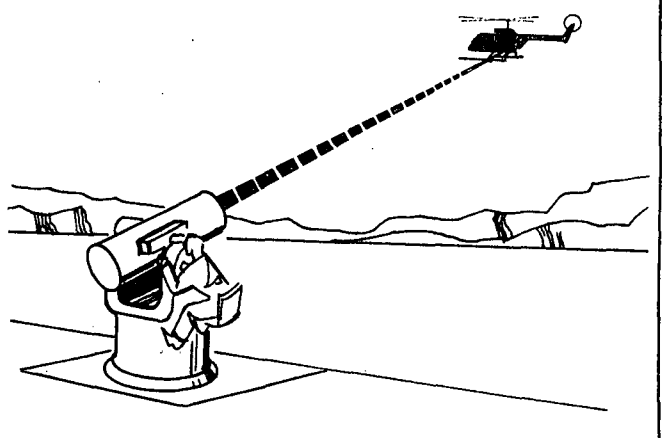

Figure 42. VERTICAL MONITOR

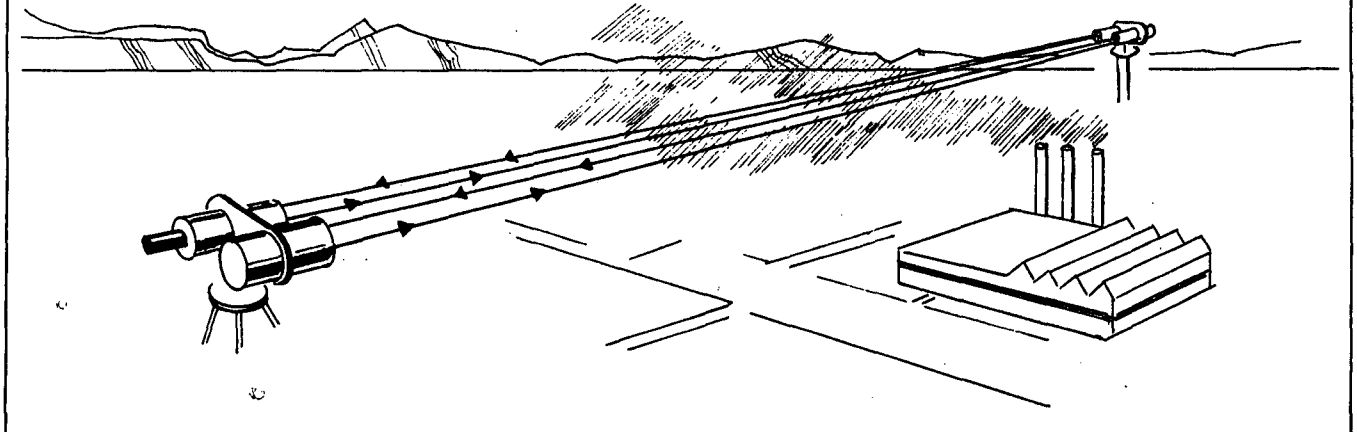

Figure 43. FOLDED PATH FOR ATMOSPHERIC STUDIES

REFERENCES

1. Bibbero, R. J., and Young, I. G., Systems Approach To Air Pollution Control John Wiley & Sons Inc., 1974.

2. Lueck, D. W. and Tschupp, E. J., "User Survey of Air Pollution Monitoring Systems," G. E. Technical Information Series Report, 72TMP-3, January 1972.

TECHNICAL REPORT DATA
(Please read Instructions on the reverse before completing)

1. REPORT NO.	2.	3. RECIPIENT'S ACCESSION NO.
EPA-600/2-77-009		

4. TITLE AND SUBTITLE
CARBON DIOXIDE LASER SYSTEM TO MEASURE GASEOUS POLLUTANTS

5. REPORT DATE
January 1977

6. PERFORMING ORGANIZATION CODE

7. AUTHOR(S)
R.J. Gillmeister and L.R. Snowman

8. PERFORMING ORGANIZATION REPORT NO.

9. PERFORMING ORGANIZATION NAME AND ADDRESS
General Electric, Ordnance Systems
Electronic Systems Division
100 Plastics Avenue
Pittsfield, Massachusetts 01201

10. PROGRAM ELEMENT NO.
1AD605

11. CONTRACT/GRANT NO.
68-02-1290

12. SPONSORING AGENCY NAME AND ADDRESS
Environmental Sciences Research Laboratory
Office of Research and Development
U.S. Environmental Protection Agency
Research Triangle Park, NC 27711

13. TYPE OF REPORT AND PERIOD COVERED
Final, May 1974-1975

14. SPONSORING AGENCY CODE
EPA - ORD

15. SUPPLEMENTARY NOTES

16. ABSTRACT

The report concerns the continuation of work in the development of a gas laser system for air pollution monitoring over long paths, a kilometer or more, using infrared absorption. Modifications to a bread-board system for simultaneous detection of O_3, NH_3, C_2H_4 and the addition of beam steering optics to give the system area monitoring capability are discussed. Operation for a two month period in St. Louis in conjunction with the RAPS program is also discussed. During this period O_3 and NH_3 were monitored at Site 103 in RAMS. Data comparing system performance with that of conventional monitors is presented along with the results of problem investigations.

17. KEY WORDS AND DOCUMENT ANALYSIS

a. DESCRIPTORS	b. IDENTIFIERS/OPEN ENDED TERMS	c. COSATI Field/Group
*Air pollution *Infrared radiation *Ozone Evaluation *Ammonia Field tests *Ethylene *Analyzers Design *Carbon dioxide lasers		13B 07B 07C 14B 20E 20F

18. DISTRIBUTION STATEMENT	19. SECURITY CLASS *(This Report)*	21. NO. OF PAGES
RELEASE TO PUBLIC	UNCLASSIFIED	111
	20. SECURITY CLASS *(This page)*	22. PRICE
	UNCLASSIFIED	

EPA Form 2220-1 (9-73)